



**PEDRO MIGUEL
XAVIER NUNES**

**TOXICITY ASSESSMENT OF METALLIC
NANOPARTICLES ON AQUATIC BIOTA**

**AVALIAÇÃO DA TOXICIDADE DE
NANOPÁRTÍCULAS METÁLICAS EM BIOTA
AQUÁTICO**

DECLARAÇÃO

Declaro que este relatório é integralmente da minha autoria, estando devidamente referenciadas as fontes e obras consultadas, bem como identificadas de modo claro as citações dessas obras. Não contém, por isso, qualquer tipo de plágio quer de textos publicados, qualquer que seja o meio dessa publicação, incluindo meios eletrônicos, quer de trabalhos acadêmicos.



Universidade de Aveiro Departamento de Biologia
2018

**PEDRO MIGUEL
XAVIER NUNES**

**TOXICITY ASSESSMENT OF METALLIC
NANOPARTICLES ON AQUATIC BIOTA**

**AVALIAÇÃO DA TOXICIDADE DE
NANOPÁRTÍCULAS METÁLICAS EM BIOTA
AQUÁTICO**

Dissertação apresentada à Universidade de Aveiro para cumprimento dos requisitos necessários à obtenção do grau de Mestre em Toxicologia e Ecotoxicologia, realizada sob a orientação científica da Doutora Isabel Maria Cunha Antunes Lopes, Investigadora Principal do CESAM – Centro de Estudos do Ambiente e Mar, do Departamento de Biologia da Universidade de Aveiro

“You know what happens when you dream of falling? Sometimes you wake up. Sometimes the fall kills you. And sometimes, when you fall, you fly.”

Neil Gaiman, *Fables and Reflections* (1993)

o júri

Presidente

Prof. Doutor Fernando José Mendes Gonçalves
Professor associado c/agregação, Departamento de Biologia, Universidade de Aveiro

Orientador

Doutora Isabel Maria Cunha Antunes Lopes
Investigadora principal do CESAM, Departamento de Biologia, Universidade de Aveiro

Arguente

Doutor Marcelino Miguel Guedes
Investigador auxiliar, Departamento de Biologia, Universidade de Aveiro

agradecimentos

Uma palavra de apreço à Doutora Isabel Lopes por ter aceite o desafio de me orientar neste trabalho. Por toda a confiança, motivação, simpatia e disponibilidade que sempre demonstrou. Um Obrigado pela experiência.

Agradeço à Cátia Venâncio por toda a ajuda na reta final deste trabalho, por ter disposto do seu tempo, pelas sugestões e bom ambiente no laboratório. Ah, e pelos podcasts!

Uma palavra de amizade à Sara, ao Bruno, Cátia, Emanuele e à Antonieta que me receberam e introduziram no grupo dos anfíbios, sempre de braços abertos e com boa disposição. Por toda a ajuda e bons momentos no laboratório.

Agradeço à Rute Pereira e ao Doutor Nuno João Silva pela disponibilidade e colaboração na realização deste trabalho. Obrigado Rute por todas as sínteses, sei que não foi fácil!

À minha família, por serem os pilares da pessoa que sou hoje, por todo o vosso apoio e presença tanto nas vitórias como nos tempos mais difíceis. Por me proporcionarem todos os dias a possibilidade de ser feliz e procurar alcançar sempre novos desafios e metas que traço para mim.

A todos os meus amigos (que felizmente são bastantes), desde os que estão mais perto, até aos que estão mais longe, porque independentemente da distância estão sempre ao meu lado e disponíveis para levantar a moral quando mais é preciso. Obrigado pelo apoio, dicas, sugestões e amizade.

E não podia deixar de agradecer também aos vários organismos que participaram (ainda que involuntariamente) nos meus ensaios, sem eles é que o trabalho não podia mesmo ter sido realizado.

palavras-chave

nanopartículas, avaliação de perigo, toxicidade, aplicações biomédicas, biota aquático.

resumo

O aumento da utilização de nanomateriais no contexto do dia a dia tem origem no desenvolvimento da nanotecnologia a partir de meados dos anos 80 do século passado, quando as suas bases começaram a ser estabelecidas. A partir daí verificou-se um enorme interesse da comunidade científica para explorar este novo tipo de materiais com propriedades interessantes e promissoras, dada a sua elevada resistência, reduzido tamanho, propriedades antimicrobianas, facilidade de síntese, entre muitas outras. Com os avanços na área, estes materiais tornaram-se comuns e com aplicações múltiplas não só nos mais variados campos da ciência, mas também da vida prática, onde começaram a integrar desde produtos de higiene pessoal, a recipientes, infraestruturas, alimentação e produtos de aplicação médica. No campo da medicina as nanopartículas de ferro têm sido muito utilizadas em técnicas no tratamento de cancro ou em simples exames de ressonância magnética. Neste contexto, o presente trabalho pretendeu avaliar a influência da composição química e tipo de funcionalização na ecotoxicidade de duas nanopartículas de ferro em organismos dulçaquícolas. Para atingir este objectivo foram seleccionadas duas nanopartículas de ferro funcionalizadas com dopamina: seleneto de ferro, $\text{Fe}_3\text{Se}_4@Dopa$, e óxido de ferro, $\text{Fe}_3\text{O}_4@Dopa$. Para avaliar a influência do tipo de funcionalização da ecotoxicidade, as nanopartículas de Fe_3Se_4 foram também funcionalizadas com levadopamina ($\text{Fe}_3\text{Se}_4@Levadopa$). Para cada tipo de nanopartícula foram realizados os seguintes ensaios de toxicidade: inibição de crescimento após 72h de exposição com a microalga verde *Raphidocellis subpacitata*, inibição de crescimento após 7 dias de exposição com a macrófita *Lemna minor*, mortalidade após 24h de exposição com o rotífero *Brachionus calyciflorus*, mortalidade, malformações inibição da alimentação após 72h de exposição com *Hydra viridissima*, e desenvolvimento embrionário após 96 h de exposição com embriões de *Xenopus laevis*. Não foi observado um padrão claro de toxicidade entre as nanopartículas. Por exemplo, as nanopartículas que apresentaram menor toxicidade para a microalga e hidra foram as de $\text{Fe}_3\text{Se}_4@Levadopa$, mas, estas nanopartículas foram também as que apresentaram maior toxicidade para *L. minor*. A espécie que apresentou maior sensibilidade a estas nanopartículas foi o rotífero *B. calyciflorus*, que apresentou mortalidade significativa a concentrações de 17.6 mg/L para as três nanopartículas. Apesar de não haver informação na literatura científica acerca das concentrações previstas ocorrerem em águas superficiais para estas nanopartículas, com base em previsões feitas para outras nanopartículas que são utilizadas em maiores quantidades em produtos de consumo humano, prevê-se que as concentrações que provocaram efeitos no presente estudo (na ordem das mg/L) estarão muito acima das que poderão ocorrer no ambiente num futuro próximo.

keywords

nanoparticles, hazard assessment, toxicity, biomedical applications, aquatic biota

abstract

The recent increase in the use of nanomaterials in the day-to-day context, is due to the emergence and development of the nanotechnology from the mid-1980s when their bases began to be established. From this point onwards, there was a great interest of the scientific community to explore this new type of material with interesting and promising properties, given its high resistance, reduced size, anti-microbial properties, ease of synthesis, among many others. With advances in this field, these materials have become of common usage and now have multiple applications not only in the most varied fields of science, but also in practical life, where they began to integrate personal hygiene products, containers, infrastructures, food and even part of biomedical techniques in the treatment of cancer or in simple MRI scans. In this context, this study aimed at evaluating the influence of chemical composition and coating in the ecotoxicity of iron superparamagnetic nanoparticles (NPs) to freshwater biota. For this, two iron NPs coated with dopamine were selected to be studied: iron (II) selenide ($\text{Fe}_3\text{Se}_4@Dopa$) and iron (II) oxide ($\text{Fe}_3\text{O}_4@Dopa$). To assess the influence of coating in the toxicity of NPs, Fe_3Se_4 was also produced with levodopamine as a coating agent ($\text{Fe}_3\text{Se}_4@Levodopa$). For each of the NPs the following toxicity assays were carried out: 72-hour growth inhibition assay with the green alga *Raphidocellis subcapitata*, 7-day growth inhibition assay with the macrophyte *Lemna minor*, 24-hour mortality assay with rotifer *Brachionus calyciflorus*, 72-hour mortality and feeding inhibition with the cnidarian *Hydra viridissima*, and 96-hour embryo development assay with *Xenopus laevis*. No clear pattern of toxicity was observed in the tested nanoparticles. For example, nanoparticles presenting less toxicity for the microalgae and hydras were the $\text{Fe}_3\text{Se}_4@Levodopa$ ones, but this was the NP most toxic for *L. minor*. The species presenting higher sensitivity for all three tested nanoparticles was the rotifera *B. calyciflorus*, exhibiting significant mortality in concentrations of 17.6 mg/L. Although there is no information in scientific literature on expected concentrations of the NPs occurring in surface waters, based on previsions performed on other nanoparticles used more commonly in human products, it is expected that concentrations that induced effects on the present study (in orders of mg/L) are far above those that may occur in the environment in the near future.

Index

List of abbreviations, acronyms and units	VI
List of figures	VII
1. Introduction	1
1.1 Contaminants of emergent concern	1
1.1.1 Which are these contaminants of emergent concern?	1
1.1.2 Contaminants of emergent concern assessment and environmental fate	3
1.1.3 Nanomaterials as a study case	5
1.2 Nanomaterials in perspective	8
1.2.1 Nanomaterials: historical context and applications	8
1.2.2 Synthesis and functionalization	9
1.2.3 Main effects and pathways	11
1.3 Medical applications of nanomaterials: the case of hyperthermia and magnetic resonance imaging (MRI) exams	14
1.3.1 Hyperthermia technique	14
1.3.2 MRI principles of operation	17
1.3.2 Contrast substances and their importance	21
1.3.4 Iron nanoparticles in hyperthermia and MRI	24
1.4 Objectives	27
2. Materials and Methods	27
2.1. Nanoparticles studied	27
2.1.1 Nanoparticles synthesis process	28
2.1.2 One-step phase exchange and functionalization	29
2.2 Model species	29
2.2.1 Producers organisms	29
2.2.2 Consumers organisms	32
2.3 Toxicological assays	38
2.3.1 Toxicological assays with producers	38
2.4 Statistical data treatment	42
3. Results	43
3.1 Nanoparticles characterization	43

3.2 Ecotoxicity assays	44
4. Discussion	52
4.1 Toxicity presenting ranges	52
5. Conclusion.....	56
Bibliography	57
Annexes	61

List of abbreviations, acronyms and units

Cm - centimeters

DBPs - disinfection by products

Dopa - dopamine

CECS – contaminants of emerging concern

EC_x - effect concentration

EDCs - endocrine disrupting compounds

ENM - engineered nanomaterials

Fe₃O₄ - iron oxide

Fe₃Se₄ - iron selenide

HP - hyperthermia

ISO - organization for standardization

L - liters

L-Dopa - levodopamine

LOEC - lowest observed effect concentration

mg - milligrams

MoA - modes of action

MRI - magnetic resonance imaging

NM - nanomaterials

NOEC - no observed effect concentration

NP - Nanoparticle

PFCs - perfluorinated compounds

PPCPs - pharmaceuticals and personal care products

SI - International units system

µg - micrograms

List of figures

Figure 1. Two-way dynamic interactions between NPs and organisms along with environmental factors	4
Figure 2. Illustration on NPs fate and possible interactions while on the environment.....	6
Figure 3. Nanoscale for comparing NMs with biological molecules	8
Figure 4. AgNPs possible interactions with surrounding cellular components	13
Figure 5. MRI machine scheme highlighting its components	21
Figure 6. Comparison between T1, T2 and flair RMI results	22
Figure 7. Dopamine molecule scheme	28
Figure 8. Levodopamine molecule scheme	28
Figure 9. Images showing cells of the microalga <i>Raphidocelis subcapitata</i>	33
Figure 10. Image of <i>Lemna minor</i> with three fronts (n)	34
Figure 11. Image of <i>Brachionus calyciflorus</i>	35
Figure 12. Image of <i>Hydra viridissima</i> organism with sprout (attached to a substrate)	37
Figure 13. Image of <i>Xenopus laevis</i> , male in the left and female in the right	38
Figure 14. Image of a <i>X. laevis</i> holding aquarium	39
Figure 15. Image of the pellets (left) and wholeworms (<i>T. molitor</i>) (right) used to feed <i>Xenopus laevis</i>	39
Figure 16. Human chorionic gonadotropin hormone vial flask	40
Figure 17. Image of <i>Xenopus. laevis</i> being injected with human chorionic gonadotropin	40
Figure 18. Neubauer chamber for cell counting illustration	41
Figure 19. Image of <i>Lemna minnor</i> assay plaque	43

Figure 20. Rotoxkit F (MicrioBioTests, Gent, Belgium) hatching kit	44
Figure 21. Toxicity in <i>Hydra viridissima</i> based on morphological changes, on a scale of scores from 0 to 10. (Source: Wilby et al. 1989)	45
Figure 22. Transmission electron microscopy images and size distribution of Fe ₃ Se ₄ (up) and Fe ₃ O ₄ (down) nanoparticles (Source: Pereira, R., 2018)	47
Figure 23. Average of specific growth rate (A) and of yield (B) of the green microalgae <i>Raphidocelis subcapitata</i> after a 3-day exposure period to three iron nanoparticles (iron selenide coated with Levodopamine – Fe ₃ Se ₄ @L-Dopa; iron oxide coated with Dopamine - Fe ₃ O ₄ @Dopa; and iron selenide coated with Dopamine – Fe ₃ Se ₄ @Dopa). Error bars correspond to the standard deviation	49
Figure 24. Average growth rate of <i>Lemna minor</i> fronds after a 7-day exposure period to nanoparticles of iron selenide coated with levodopamine (Fe ₃ Se ₄ @L-Dopa). Error bars correspond to the standard deviation. * indicates significant differences relatively to the control (Dunnett's, p<0.001)	50
Figure 25. Average growth rate in <i>Lemna minor</i> fronds after a 7-day exposure period to two iron nanoparticles (iron oxide coated with Dopamine - Fe ₃ O ₄ @Dopa; and iron selenide coated with Dopamine – Fe ₃ Se ₄ @Dopa). Error bars correspond to the standard deviation. * indicates significant differences from the respective control (Dunnett's, p<0.05)	51
Figure 26. Survival assessment of <i>Brachionus calyciflorus</i> after a 24-h exposure period to three iron nanoparticles (Iron selenide coated with Levodopamine – Fe ₃ Se ₄ @L-Dopa; and Iron oxide coated with Dopamine - Fe ₃ O ₄ @Dopa). Error bars correspond to the standard deviation; *indicates significant differences relatively to the respective control (Dunnett's; p<0.05)	52
Figure 27. Percentage of malformations in <i>Hydra viridissima</i> after a 96-h exposure period to iron selenide coated with Dopamine - Fe ₃ Se ₄ @Dopa	53
Figure 28. Images of <i>Hydra viridissima</i> ; a) healthy <i>Hydra viridissima</i> hydranth; b to d) malformations detected on <i>Hydra viridissima</i> hydranths exposed to iron selenide nanoparticles coated with dopamine (Fe ₃ Se ₄ @Dopa) at a concentration of 88 mg/L. Red arrows represent cubbed tentacles and loss of endosymbiotic algae cells and the yellow arrow represent loss of endosymbiotic algae cells at the foot of the hydranth The image was taken with a Leyca magnifier with an ampliation of 400x times	53

Figure 29. Average percentage of feeding inhibition of *Hydra viridissima* after a 96-h exposure period to three iron nanoparticles (iron selenide coated with levodopamine – Fe₃Se₄@L-Dopa; iron selenide coated with dopamine - Fe₃Se₄@Dopa; and iron oxide coated with dopamine - Fe₃O₄@Dopa). Error bars correspond to the standard deviation. * indicates significant differences relatively to the respective control (Dunett's; p<0.05)..... 54

Figure 30. Average percentage of mortality of *Xenopus laevis* embryos after a 96-h exposure period to the nanoparticle of iron selenide coated with Levodopamine (Fe₃Se₄@L-Dopa). Error bars correspond to the standard deviation 55

Figure 31. Average percentage of mortality of *Xenopus laevis* embryos after a 96-h exposure period to the nanoparticle of iron oxide coated with Levodopamine (Fe₃O₄@L-Dopa). Error bars correspond to the standard deviation 55

Figure 32. Embryos of the African clawed frog *Xenopus laevis* after exposure to iron oxide nanoparticles coated with levodopamine (Fe₃O₄@L-Dopa) at the following concentrations: a) 19.7 mg/L; b)66 mg/L; c) and d) 100 mg/L. 1. Jelly coat that surrounds the egg; 2. Embryo. Black arrows pointing to nanoparticles adsorbed to the eggs jelly coat 56

1. Introduction

This first chapter will provide a general introduction on emergent contaminants, including their fate on natural matrixes and environmental effects. It will focus more specifically nanomaterials, by addressed their applications, synthesis and characterization methods, prospective works and some feasible future utilizations. Will also be presented the specific application for the nanomaterials that were studied in the present work, iron oxide and iron selenide nanoparticles (Fe_3O_4 and Fe_3Se_4) with assorted coatings in Magnetic Resonance Imaging (MRI) radiological exams, general modes of action and adverse effects on biota, and further results on the practical toxicology study that they were subjected to, as well as an overview of the organisms utilized within the latter.

1.1 Contaminants of emergent concern

1.1.1 Which are these contaminants of emergent concern?

Environmental quality criteria are based in any type of changes experienced by the environment, either from anthropogenic sources or natural ones, often reporting to water, soil or air quality. When an ecosystem experiences degradation (in a biological, chemical or physical level) often caused by human activities, its characteristics like structure, processes, are influenced, which decreases its resilience. Ecosystems have been identified to be impacted with contaminants of emerging concern (CECs), compounds that are now being detected in the environment or that their frequency increased recently (Wu, L. et al., 2011) As a new compound begins to cause environmental concerns, even after approval by regulatory entities (like European Chemical Agency – ECHA), data accumulate on its environmental chemistry, ecotoxicological and human toxicity, as well as its epidemiology. This eventually results in government action to establish environmental guidelines or criteria to ensure adequate protection. In a similar sequence, compounds that are already regulated are often re-evaluated with the addition of new data.

Reasons for toxicity evidencing after testing may be related with environmental relevant concentrations, byproducts originating from organismal metabolism (in pharmaceutical uses p.e.) or other processes. This eventually results in international entities to act into establish environmental guidelines or criteria to ensure adequate protection. In a similar sequence,

compounds that are already regulated are often re-evaluated with the addition of new data, if possible (ECHA, 2018)

A large number of CECs have already been found in environmental matrices with a wide diversity of characteristics, such as their potential biotoxicity, bioaccumulation, and persistence in the environment. However, standard monitoring and regulatory programs have not covered most of these novel contaminants. The CECs group includes a large diversity of chemicals such as pharmaceuticals and personal care products (PPCPs), endocrine disrupting compounds (EDCs), perfluorinated compounds (PFCs), flame retardants, industrial additives, disinfection by products (DBPs), algal toxins, among many others (Khalid, S. et al., 2018). The difficulties in the chemical analysis and characterization of CECs lie mainly in the complexity of environmental matrices, the extremely low environmental levels (usually at ppb to ppt levels), and their emerging nature (lack of basic knowledge on them) (Huang, Liu, Yao, & Jiang, 2017).

Contaminants of emerging concern have been identified in soil irrigated with reclaimed water, accumulate in fish inhabiting areas that receives wastewaters from treatment wetlands, and to disrupt cellular development and hormonal function in sheep reared on sewage sludge treated pasture (Khalid, S. et al., 2018). Complex mixtures of CECs at environmentally relevant concentrations were reported to inhibit the growth of human embryonic cells and to produce significant effects at the molecular level even at levels below no observed effect concentrations (NOECs). The occurrence of some CECs (e.g. synthetic hormones, like estrogens) correlates with ecological effects and sexual abnormalities in fish (Vigilino, A. et al., 2008). There is also evidence that some CECs are persistent in the environment and also persist through conventional water treatment processes representing a potential concern to public drinking water supplies utilizing water resources that contain CECs (Vigilino, A. et al., 2008).

The large number of CECs poses a challenge for regulatory agencies. How to prioritize research about CECs? How to prioritize the definition of quality criteria or norms for all of these new substances for which we generally have only sparse knowledge on their behavior in the environment or on their toxic effects on the environment?

1.1.2 Contaminants of emergent concern assessment and environmental fate

The release of chemicals into the environment may lead to their presence in the air (e.g. due to their volatilization and dust emissions), surface water (e.g. direct release into water bodies, surface runoffs or overland flow), groundwater (e.g. through infiltration), soils (e.g. due to erosion - including dust generation and deposition), sediments (e.g. from surface runoff), and biota (e.g. through uptake and bioaccumulation). The distribution of contaminants in the environment is influenced by a complex set of processes including transport, transformation, degradation and decay, inter-media transfer, and biological uptake (Hotze, E. et al., 2010). In addition, many of these compounds are persistent and undergo complex interactions in more than one environmental matrix. Environmental fate analyses can be used to assess the movement of chemicals between environmental compartments. The fate of chemical compounds that are released into the environment forms an important basis for evaluating the exposure of biological receptors to hazardous chemicals. Multimedia transport models are generally employed in the prediction of the long-term fate of such chemicals in the environment (Hotze, E. et al., 2010).

The potential for inter-compartment transfer of contaminants, namely from the soil to other compartments is particularly significant - in fact, contaminated soil can be a major source for the contamination of groundwater, atmospheric air, subsurface soil gas, sediments, and surface water (Verdier, A. 2009). For example, chemical constituents having a moderate to high degree of mobility can leach from soils into groundwater. Conversely, the potential for inter-compartment transport of constituents into soils does also exist, for example, chemicals may be transported to soils via atmospheric deposition, and also through releases of subsurface gas.

The affinity that contaminants have for soil particles affects the rate of their mobility and transport. For instance, hydrophobic or cationic contaminants are known to migrate more slowly throughout the soil. Adsorption to soil or sediment particles may also contribute to a lower transport rate of chemicals in the environmental matrices. On the other hand, a number of natural processes work to lessen or attenuate contaminant concentrations in the environment - the mechanisms of natural attenuation include dispersion and dilution, ion exchange, precipitation, adsorption and absorption, filtration, gaseous exchange, and biodegradation. The partitioning of inorganic chemicals is somewhat different from organics. Typically, metals

generally exhibit relatively low mobility (Yang & Yu, 2002). The inorganics will tend to adsorb onto soils (which may become airborne or be transported by surface erosion) and sediments (that may be transported in water) (Verdier, A. 2009). A scheme of some of the interactions a nanoparticle (one of many CECs) can experience on an environmental matrix is portrayed in Figure 1.

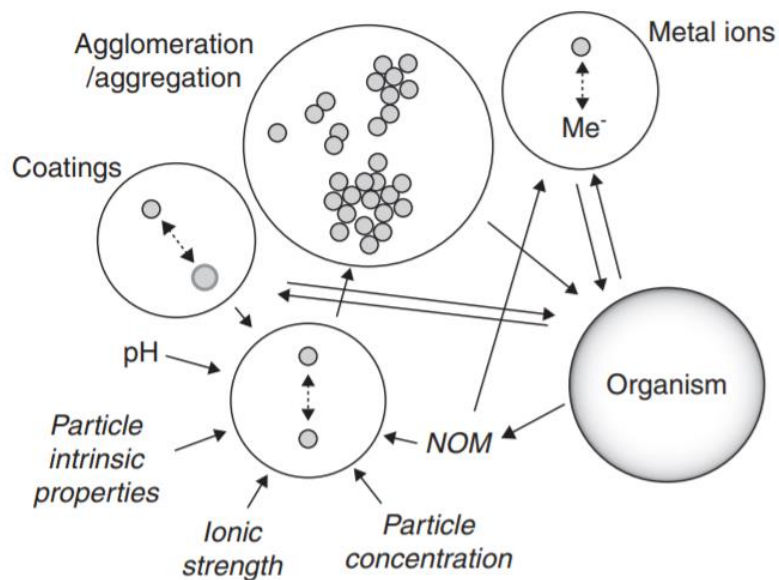


Figure 1. Two-way dynamic interactions between nanoparticles and organisms along with environmental factors; NOM – natural organic matter (Source: Hartmann, 2012).

Most environmental long-distance transport of chemicals occurs through air or water. In these compartments, there are primarily two kinds of physical processes by which chemicals are transported: via bulk movement of fluids from one location to another, and via random (or seemingly random) mixing processes within the fluids (Yang & Yu, 2002). Both types of mass transport processes are implicitly included in the input and output transport terms. The first type of process, advection, is due to bulk, large-scale movement of air or water, as seen in blowing wind and flowing streams. In the second type of transport process, a chemical is moved from one location in the air or water where its concentration is relatively high to another location where its concentration is lower, due to random motion of the chemical molecules (molecular diffusion), random motion of the air or water that carries the chemical (turbulent diffusion), or a combination of the two (Amatore, C. 2015).

Although exhaustive, answering questions like the following ones is key to better comprehend chemicals behavior and how to effectively treat, set regulatory guidelines, manipulate and discard this kind of materials that will provide adequate protection to ecosystems as well as to human health. Here are some examples of such questions for a specific type of CECs, the nanomaterials (NMs) – Do biota, such as biofilms and invertebrates, modify the behavior of nanomaterials (NMs)? Do they retain their nominal nanoscale size and original structure and reactivity in aquatic and soil/sedimentary systems? Are most of the contaminants persistent, while being mobile in the environmental matrices, or are they easily degradable and have low mobility? Do they present by-products more toxic than their original form? An illustration of the probable interactions that nanomaterials (NMs), a type of CECs, goes through in the environment is represented in Figure 2.

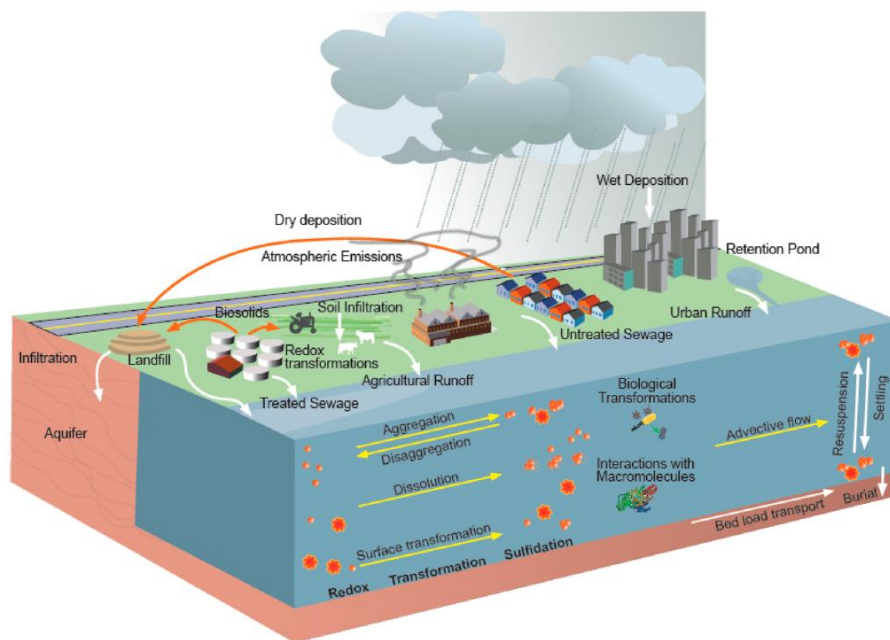


Figure 2. Illustration on NMs fate and possible interactions while on the environment. (Source: (Dale, A. et al., 2015).

1.1.3 Nanomaterials as a study case

Nanomaterials (NMs) constitutes a group of CECs that have raised environmental concerns since they exhibit unique properties that may influence their fate and effects in the environment. The production of NMs represent an active area of scientific research, industrial applications and are

quickly rising in a techno economic sector with full expansion in many application domains. The NMs have gained prominence in technological advancements and nowadays nanotechnology is considered one of the six key enabling technologies of Europe (European Commission, 2016) as it presents growing prospects for the development of inventive products and applications in a wide array of sectors, including medical and pharmaceutical sectors to electronics, food processing, agricultural productions, among others. These materials gained such promising status due to their tunable physicochemical characteristics such as melting point, wettability, electrical and thermal conductivity, catalytic activity, light absorption and scattering, resulting in enhanced performance over their bulk counterparts, applied in many areas of human activities (Gaffet, 2011).

A nanometer (nm) is an International System of Units (SI) unit that represents 10^{-9} meters in length (Fig. 3). Nanomaterials are described as materials with length of 1–100 nm with at least one dimension – despite that, they are commonly defined to be of diameter in the range of 1 to 100 nm (ISO, 2015). Today, there are several pieces of legislation in the European Union (EU) and in the United States of America (USA) with specific references to NMs – nonetheless, a single internationally accepted definition for NMs does not exist. Different organizations have different opinions while defining these materials. The International Organization for Standardization (ISO, 2010) has described NMs as a “material with any external nanoscale dimension or having internal nanoscale surface structure”.

Likewise, the term nanomaterial is described as “a manufactured or natural material that possesses unbound, aggregated or agglomerated particles where external dimensions are between 1–100 nm size range”, according to the EU Commission - Nanofibers, nanoplates, nanowires, quantum dots and other related terms have been defined based on these definitions (European Commission, 2016). The use of various interpretations across different jurisdictions acts as a major handicap to regulatory efforts as it leads to legal hesitation in applying regulatory approaches for identical materials. In the EU, engineered NM in food products have been defined as “any intentionally produced material that has one or more dimensions of the order of 100 nm or less or that is composed of discrete functional parts, either internally or at the surface, many of which have one or more dimensions of the order of 100 nm or less, including structures,

agglomerates or aggregates, which may have a size above the order of 100 nm but retain properties that are characteristic of the nanoscale” (European Parliament and Council, 2015).

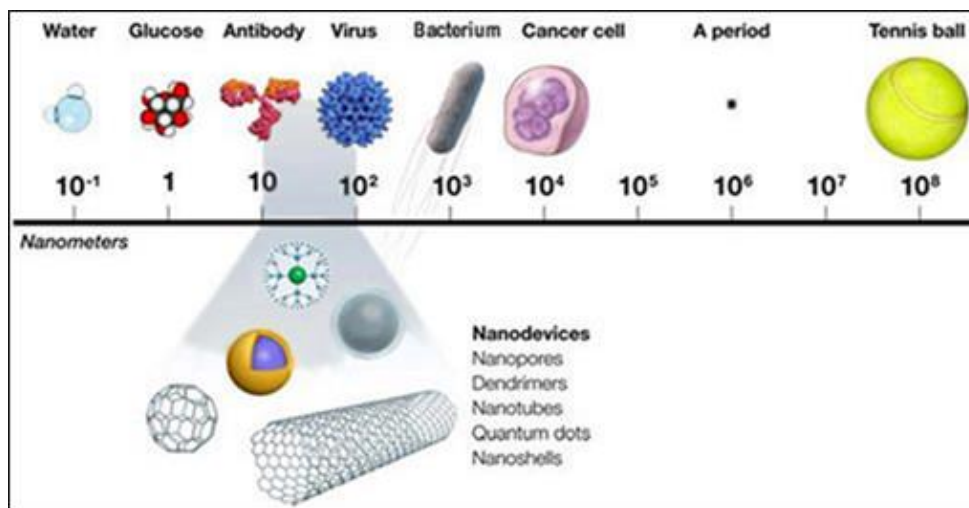


Figure 3. Nanoscale for comparing NMs with biological molecules. (Source: introtonanotechnology.weebly.com/the-nanoscale.html)

Most current NMs can be organized basically in four categories based on its materials (Gaffet, 2011): the first ones are carbon based NMs where these NMs are constituted by carbon, and can be found in morphologies like hollow tubes, ellipsoids or spheres - carbon nanotubes, nanofibers, and graphene are examples of the most synthesized among this category. Second, there are the inorganic based NMs: often include metals (like Ag) and metal oxide (TiO_2 or ZnO , among others) and other elements or materials (such as semiconductors like silicon and ceramics per example). The third group consists of organic based NMs, which are made essentially of organic matter, excluding carbon based or inorganic based NMs - the utilization of non-covalent (and so, weak) interactions for the assembly and design of molecules helps to transform these organic materials into desired structures such as micelles, polymer NMs, liposomes or dendrimers. The last category is the composite based NMs group, which are multiphase, with one phase on the nanoscale dimension that can either combine nanoparticles (NPs) with each other or NPs combined with larger materials or even with bulk ones (like nanofibers). The composites may be any combinations of carbon based, metal based, or organic based NMs with any form of metal, ceramic, or polymer bulk materials. These kinds of materials can present one, two, or three dimensions, in the nanoscale regime.

Nanomaterials can also be classified based on their origin (Gaffet, 2011). Firstly, natural NMs, which may be produced by biological entities or physical processes (e.g. erosion). These naturally occurring NMs are ubiquitous on Earth's, they occur in the hydrosphere, atmosphere, lithosphere and even in the biosphere, regardless of human actions. The second groups are synthetic (or laboratory engineered) NMs that are produced by human activities through several physical, chemical, biological or hybrid techniques (e.g. mechanical grinding, engine exhaust and smoke production).

Finally, in terms of sources of NMs there are three main categories (Gaffet, 2011). Firstly, the incidental NMs, which are produced incidentally as a byproduct of industrial processes (such as NMs produced from vehicle engine exhaustion, welding fumes, combustion processes and even some natural process such as forest fires). The second ones are engineered NMs, which have been manufactured by humans to have certain required properties for desired applications (simple combustion during cooking, in vehicles, fuel oil and coal for power generation, ore refining) - materials such as carbon or TiO_2 NPs, per example. The third group is the naturally produced NMs, which can be found in the bodies of organisms, insects, plants, animals and human bodies. However, the distinctions between naturally occurring, incidental, and manufactured NPs are often blurred. In some cases, for example, incidental materials can be considered as a subcategory of natural ones. One of the main differences between incidental and engineered is that the morphology of engineered NMs can usually be better controlled as compared to incidental. Also, engineered NMs can be purposely designed to exploit novelty features that derive from their smaller size (Gaffet, 2011).

1.2 Nanomaterials in perspective

1.2.1 Nanomaterials: historical context and applications

In 1857, Michael Faraday reported the synthesis of a colloidal Au NM solution, which is the first scientific description to report these NMs preparation, and so initiated the history of NPs in the scientific area. He also revealed that the optical characteristics of Au colloids are dissimilar compared to their respective bulk counterpart. In the 1940s, SiO_2 NPs were manufactured as substitutes to carbon black for rubber reinforcement. Today, manufactured NMs can significantly improve the characteristics of bulk materials, in terms of strength, conductivity, durability, and

lightness, and they can provide useful properties (e.g., self-healing, self-cleaning, anti-freezing, and antibacterial) and can function as reinforcing materials for construction or sensing components for safety. Per example, their potential to improve quality of life is enormous - nanomedicine is helping to provide better targeted therapies, polymer nanocomposites are providing lighter, stronger materials and advanced membrane technologies. Nanotechnologies also hold great promise for using resources more sparingly, providing potable water, and improving the efficiency of energy production and use. Nanoparticles also feature in many consumer products such as electronic components, cosmetics, cigarette filters, antimicrobial and stain-resistant fabrics, as batteries, paints, wound dressings, food additives, personal care products, and even in pesticides. Indeed, no less than 15 % of all global consumer products are estimated to be nano-labeled. Nanoparticles have also been employed in environmental remediation to improve the quality of air, water and soils. Per example, magnetic iron oxide NMs have been used to remove arsenic from drinking water (Khot, L. et al, 2012). The ions adsorb on the NM surface and then a magnetic field is used to separate the complex from the water. Given the absolute and increasing scale of production of NPs allied to their uncertain effects on human health and the environment it is important that the presence of these compounds in the environment can be measured and monitored along with their chemical identification and concentration. The quantification of these materials in the environment represents a significant analytical challenge.

The more frequent use of these materials in consumer goods and industrial sectors also means their occurrence in the biosphere will continue to grow. The magnitude of the challenges in predicting the environmental behaviors and potential effects of NMs is daunting given the tremendous diversity of them already in production, thus reinforcing the need for testing and regulation on the use of these novel materials.

1.2.2 Synthesis and functionalization

Numerous synthetic methods have been developed for the production of NMs, such as thermal decomposition/reduction, coprecipitation, hydrothermal, microemulsion, and sol-gel synthesis (Shi, S. et al., 1999). These methods control the assembly of NMs by putting together atoms from precursors and are widely used to synthesize NMs with adequate control of size and morphology.

In the following sequence will be given highlights to the synthesis method chosen to synthesize the studied NPs.

Thermal decomposition methods imply the synthesis of hydrophobic nanoparticles, which can be considered a disadvantage for biomedical applications (Ali, A. et al., 2016). Hence, it is necessary to perform a hydrophobic-hydrophilic phase exchange or some sort of surface coating, so these particles can be dispersed in dilution media or when in biomedical applications, in the blood (as it is water-based) and increase their efficient biodistribution. Often, surface coatings are used to achieve a specific functionalization (Patil, R. et al., 2018). Functionalization strategies usually consist on a first step, which aims at covering the surface with reactive groups (amino, carboxylates, thiols, aldehydes) to ensure, at the second step, the further coupling of biomolecules of interest, such as streptavidin or antibodies. Some strategies include polymers, proteins, protein-resistant MR probes and hyaluronic acid layers (Smolensky, E. et al., 1999). Although, these surface coatings are usually thick, which increases the total radius of the NMs. Specially in biomedicine, the size of NMs can affect the success of its application. Thus, it is common to look for alternatives that allow: (1) a simple functionalization method and (2) a coating that does not increase much the size of the NM (Zvarec, O. et al., 2013). As an example, scientists have developed catechol-based biomolecules to anchor onto the surface of NM (Chen, J. et al., 2014; Wang, W. et al., 2016). This strategy relies on the chemical anchoring of hydroxyl groups (-OH) onto the surface of Fe_3O_4 NMs, leaving different organic groups at the surface available for further linkages. For example, in the case of caffeic acid, the NM would be functionalized with carboxylic groups (-COOH), whilst in dopamine would be functionalized with amines (-NH₂). This allows the possibility of a one-step phase exchange and functionalization with small biomolecules, decreasing the time and resources used in these processes when compared with the typical two-step method. Although, these methods tend to use organic solvents (tetrahydrofuran), which should be avoided as possible, following the Green Chemistry principles as a way to reduce toxicity of the final product and the obtained waste (Winterton, N. 2016).

Most synthesized NM have a hydrophobic surface and will aggregate and precipitate quickly if not stabilized, for this reason coating particles are added to their surface. The coating of NMs

that are used for biomedical purposes in addition to promoting their stabilization also facilitates their biocompatibility and interaction with biological membranes. In this case, surface interaction with biological molecules produces an aggregate of proteins and ions at the surface of the NM.

1.2.3 Main effects and pathways

Many NMs are produced for medical use. In addition to their beneficial effects some adverse effects may occur. Upon entrance into the blood circulation, NM use the bloodstream to reach different body compartments and organs such as the liver and spleen. In the spleen, NMs are captured by the cells of the reticuloendothelial system (RES), which is a process that is essential for the deactivation and elimination of foreign bodies (Liu et al., 2008). Other vital organs of the human body that NMs reach include the brain and the testis or even the fetus. Per example, positively-charged NMs have the ability to easily enter the cell wall (contrarily to negatively-charged ones) that consists in a double layer of phospholipids, since it is negatively charged – hence, the raise in the uptake of positively charged (also cationic) NMs could result in augmented damage to the membrane lipids as well as to cellular compartments, like the lysosomes (Xia et al., 2006).

An *in vitro* study by Rybski et al., 1991, studied how silver nanoparticles may enter the cells, reporting phagocytosis and passive diffusion through the cell membrane as the most probable processes. Once inside the cell cytoplasm, they can be visible in intracellular vesicles and are able to enter organelles like mitochondria and nuclei. The entry of silver nanoparticles into cells and their toxic potential once again appear to be size dependent (Fig. 4).

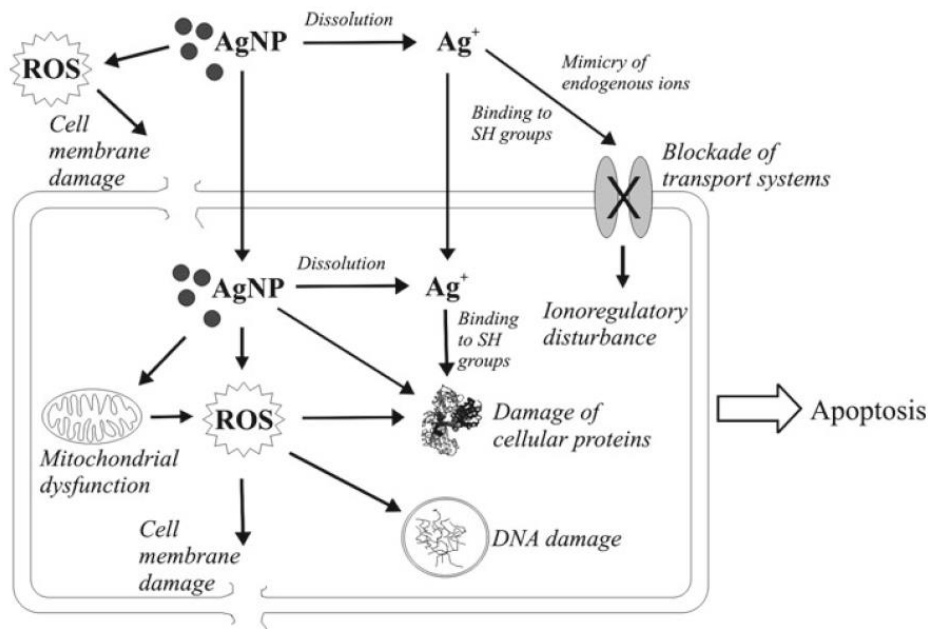


Figure 4. AgNPs possible interactions with surrounding cellular components (Source:(Völker, C. et al., 2014))

Several works have been developed aiming to evaluate the mode of action (MoA) and toxicity of NMs, from the cell to the individual level. However, conflicting results have been reported regarding size and coating-dependent toxicity and biokinetics *in vitro* and *in vivo*, and thus, basic questions regarding whether NMs (ranging from 1 to 100 nm in size) are comparatively more toxic than larger-sized particles remain unanswered. This may be closely associated with changes in physicochemical properties of NMs in biological fluids. Understanding *in vivo* physiological barriers, biological fates, and absorption mechanism of NMs upon exposure routes will be useful to predict their toxicity potential.

Nanomaterials have intrinsic properties that might increase their toxicity potentiality comparatively to their bulk counterparts, these include: particle size, surface area and charge, shape and structure, solubility, and surface coatings (Gatoo et al., 2014). Small size of NMs increases surface area per unit mass, and this surface area is often correlated with higher biological reactivity (Bakand, S. et al., 2012).

Many published works have reported that exposure to NMs leads to the formation of free radicals such as superoxide anion or hydroxyl radical, causing oxidative stress in biota (Bakand, S. et al., 2012). Overproduction of reactive oxygen species (ROS) activates the immune system

cells like cytokines, interleukins and tumor necrosis factor (TNF) as an index to present proinflammatory signaling processes - a mean to counter the latter processes. Often these result in cell apoptosis induction. After the cell phagocytosis of the NPs, macrophages are activated to release considerable amounts of oxygen radicals, proinflammatory mediators and proteolytic enzymes (also growth-regulating proteins). These inflammatory processes can also result in edemas, macrophages accumulation and pneumocyte apoptosis (Brohi, R. et al., 2017).

The production of ROS may also be linked with genotoxicity. Some studies have reported that long-term inflammation and oxidative stress may induce DNA damage in cells and tissues (Rim, K. et al., 2013). Also, continuous ROS production in the cell can cause gene mutations/deletions leading to mutagenesis, carcinogenicity, and subsequently development of tumors and cancer - particularly the metal-based ones like Ag, Au or TiO₂ NMs (Rim, K. et al., 2013).

However, the molecular mechanisms underlying nanotoxicity are not entirely understood specially because the variety of NMs being produced and commercialized is very high. Although, because it is well established that oxidative stress is a key determinant of NPs induced injury, the characterization the ROS response resulting from NPs is necessary - a better physic-chemical characterization and understanding of the multiple signaling cascades activated by NPs induced ROS, will contribute to NP-induced injury studies.

Other effects that have been reported following exposure to NMs involve disruption of male and female mammals reproductive system (Brohi, R. et al., 2017), regulate the expression of some metabolic genes, inhibit the formation of bacterial biofilms cell apoptosis, neurodegenerative abilities (AgNPs exhibit functional disruption of the blood brain barrier (BBB) following brain edemas formation (Deatsch, A. & Evans B., 2014). Long-term *in vivo* studies in murine models have shown that small NMs often accumulate in the spleen and organs like the brain, the liver, lung tissues, and even in the uterus and uterine wall (Ruiz, 2015).

Regarding iron oxide NPs, they have been used in diagnostic, biomedical and drug delivery fields and have been found to accumulate mainly but not only in the liver but also other organs, like the lungs, spleen and brain (evidencing their ability to cross the BBB). *In vivo* studies have shown that after entering the cells, these NPs remain in cell organelles (endosomes or lysosomes) being released into cytoplasm after decomposing and contributing to the cellular iron poll (Bahadar, H.

et al., 2016). Evidence show that these NPs exert their toxic effect in the form of cell lysis, inflammation, and disturbing blood coagulation system. Reduced cell viability has also been reported as a common toxic effect in *in vitro* studies. Iron oxide NPs coated with different substances have shown variable cell viability results – low concentrations (25-200 µg/mL) of these NPs coated with Tween (a surfactant) present more cell toxicity than higher concentrations (300-500 µg/mL) in murine macrophages as found by Naqvi *et al.* 2013, while in other studies on mouse neuroblastoma cell lines (Neuro-2A), the same nanoparticles have been found to present less toxic effects in terms of cell apoptosis, morphology and permeability but also mitochondrial functions, when presented in concentrations from 10 µg/mL to higher than 200 µg/mL (Jeng & Swanson, 2006). In relation with iron selenide, there is still a lack of literature reviews on its toxicity, besides existing some papers on their synthesis.

1.3 Medical applications of nanomaterials: the case of hyperthermia and magnetic resonance imaging (MRI) exams

1.3.1 Hyperthermia technique

The first report of heat being useful in cancer treatment was made by Busch (1866), who reported the disappearance of a sarcoma after a high fever event, caused by a skin disease named erysipelas. Bruns (1887) later reviewed several cases of tumor regression after fever was introduced in literature, where there are many reports in the early 1900s of the use of applied heat in treating cancer (Wust P. et al., 2002). The National Cancer Institute from United States of America, defines this therapeutic technique as hyperthermia: “*A type of treatment in which body tissue is exposed to high temperatures to damage and kill cancer cells or to make cancer cells more sensitive to the effects of radiation and certain anticancer drugs*” (NCI, 2018).

So basically, hyperthermia's a therapeutic procedure used to raise the temperature of a region of the body affected by cancer. It is applied together with other medical treatment modalities, from surgery to radiotherapy, chemotherapy, gene and immunotherapy, to name a few, and it can even enhance the effects of certain anticancer drugs. Direct cell killing temperatures are located at temperatures ranging from 41 to 48°C, where temperatures are maintained for about one hour or more during treatments. (Wust, et al., 2002). Above these temperatures it is not feasible, because heat itself is lethal to cells *in vitro*, as their survival decreases exponentially in

relation of exposure time. However, the thermal dose response relation varies among cell lines and also depends, on microenvironmental factors, mainly pH. A synergistic interaction between heat and radiation dose as well has been validated in preclinical studies. There are innumerable targets in the cell affected by the rise in temperature that have been found, such as membranes, the cytoskeleton, synthesis of macromolecules, and DNA repair. The expression of several genes can be upregulated or downregulated by heat, for example, the family of heat-shock proteins (Rentchnick, P., 1987). Expression of other genes modulated by heat it may be possible, but it is yet to be discovered (Wust, P. et al., 2002). The temperature increment required to perform the technique can be achieved by various methods including microwaves, radio waves, ultrasounds hot water perfusions, among others (Laurent, S. et al., 2011).

Although these techniques are able to increase the intracellular temperature up to the cellular death, additionally they can provoke harmful side effects such as ionization of the genetic material or lack of selectiveness in radiation and microwaves therapies, respectively, that affect the surrounding healthy tissues. This encouraged the search of new mechanisms capable of increasing the temperature of damaged areas while keeping the rest of tissues healthy. Recently nanotechnology has raised to provide a novel and original solution to these problems cited above, presenting the magnetic hyperthermia technique (MH)(Lauren, S. et al., 2011).

Magnetic hyperthermia allows to remotely induce local heat by means of magnetic energy losses of magnetic nanoparticles (NPs) under an external oscillating magnetic field, through changes in internal magnetic moment. In other words, the ability of some magnetic NPs to transform the electromagnetic energy into heat allows the temperature increase in well-defined regions in the human body where the tumor cells and these particles conjugate. Therefore, the activation of these NPs as nano heaters can be controlled externally by applying or removing an oscillating magnetic field. The electromagnetic radiation used in magnetic hyperthermia generally ranges between several kHz and 1 MHz in the radio frequency - measuring the specific absorption rate (SAR) quantifies the heating efficiency. This radiation is completely innocuous and presents enough penetration depth to access inner organs or tissues in the body. The specificity of this technique is achieved by the higher sensitivity of the tumoral cells to temperature increases

above 42°C, temperatures at which the natural enzymatic processes that keep the cells alive are disrupted, allowing their selective killing (Laurent, S. et al., 2011).

Magnetic hyperthermia is based on the injection of magnetic NPs colloidal suspension (which are excellent heat conductors) that accumulates at the tumor area either passively (by the enhanced permeability and retention (EPR) effect, extravasating from immature blood vessels) or actively (using ligands at NPs surface, specific for the surface receptors present on cancer cells), where they are then cleared by circulating macrophages and resident reticuloendothelial cells, located in the spleen and the liver (Ho, D., 2014). The use of magnetic NPs is suggested as a relatively non-toxic method for cancer treatment. In this context, magnetic hyperthermia rises as a new cancer therapy in vivo with some advantages over the traditional ones – the small size of the particles acquiesces them to pass through the biological barrier, being less invasive, homogeneously heating every point of the tumor (depending on tumor's size and depth) and NPs applied to hyperthermia can be also used as contrast agent for MRI (Laurent, S. et al., 2011).

Depending on the treatment and tumor the time period that NPs need to be in contact with the tumor may be longer, therefore it is important to study mechanisms where NPs can accumulate and be stable without clearance for a certain time window frame. One common method to evade capture (subsequently excretion) is to functionalize the surface of particles with substances that render them some properties – these are commonly functionalized with hydrophilic and biocompatible materials which are protease resistant, non immunogenic and non antigenic, such as polyethylene-glycol (PEG), dextran or chitosan per example (Behrouzki, Z. et al., 2016). The resulting increase in circulation time allows greater EPR mediated passive accumulation in tumors. On other hand, a key factor for such biomedical applications, is magnetic is the superparamagnetic behavior that NPs may exhibit, this means that the magnetization drops to zero when the applied magnetic field is removed (Kaur et al., 2017). This fact implies that neither coercive forces or remanence ones exist, preventing magnetic interactions between particles and their aggregation, which could lead to serious adverse problems derived from the formation of clots in the blood circulation system (Laurent, S. et al., 2011).

There are although some persisting challenges in NP based hyperthermia treatments, namely biocompatibility and scale-up and heterogeneity of biodistribution. In relation to biocompatibility

there is the need to develop novel non-toxic NPs besides the ones already in use, and better refine their production mechanisms, in order to optimize the yield (Kaur et al., 2017). Regarding biodistribution, a suitable balance should be found between NPs size distribution and their magnetic properties, because NPs that are too small could not show hyperthermia effect whereas bigger NPs could not be able to cross the endothelial barrier through the continuous capillaries.

As iron oxide NPs are being utilized on this field, there has been developments of suspensions for administration on patients – Per example, regarding Fe_3O_4 , a formulation of 12nm NPs coated with aminosilane has been clinically tested by a German company named MagForce® AG, where approximately 5mL of the fluid is injected directly in patients' glioblastomas whose are then subjected to a treatment twice a week with 100kHz while receiving 30Gy of radiation therapy at 2Gy per fraction. This formulation presents great promises for hyperthermia technique application on deep tumors and has demonstrated a median overall survival of 13.4 months in glioblastoma patients, contrary to the typical median survival of about 6 months - so more than the double time, while even with minimal toxicity. Reported inconvenient manifestations include fever, sweating, tachycardia and convulsion (Tu, C. et al., 2011). In the case of iron selenide (Fe_3Se_4) there's still a lack of information on these NPs usage as an HP agent.

1.3.2 MRI principles of operation

Magnetic resonance imaging (MRI) was first introduced to the scientific community by Paul Lauterbur (1973), when he published images representing the nuclear magnetic resonance (NMR) response of hydrogen nuclei in a pair of water labeled glass capillaries. One dimensional projections of this response were first obtained through a procedure that involved applying static magnetic field gradients to the sample, mapping NMR frequency into the source position. A series of one dimensional projections, acquired along different gradient directions, were then combined to reconstruct a two dimensional image. Lauterbur's simple but insightful demonstration launched a wave of scientific, industrial, and clinical activity that has since then profoundly influenced the practice of medicine. The latter technique is based in NMR fundamentals as a quantum mechanical phenomenon – it deals with physical dynamic of

microscopic objects (more precisely atomic nuclei) that behave after well understood laws of quantum mechanics.

The NMR phenomenon was first described experimentally by Bloch and Purcell in 1946, for which they were both awarded the Nobel Prize for Physics in 1952. The technique has rapidly evolved since then, following the introduction of wide superconducting magnets, allowing development of clinical applications. The first clinical magnetic resonance images were produced in England in 1980, turning this technique an accessible, widely available and powerful clinical tool. Based on this, MRI's a technique often utilized within medical practices to evaluate conditions in the human body, as abnormalities, tumors and other conditions, through the production of radiological images, based on the latter one. It uses signals transmitted by protons (usually hydrogen nuclei in water from the patient body) to create depth sensitive radiological images through a scheme of gradient tonalities of white, black and grey colors. Although the most commonly imaged nucleus in clinical practice is hydrogen (H^+), because of its great abundance in the human body (found in the form of water throughout the body), there are other nuclei that could be used in MRI includes carbon (C), phosphorus (P) sodium (Na) and even deuterium (2H) (Taouli et al, 2010).

When unperturbed in a static magnetic field, nuclei with magnetic spins are in equilibrium: an almost an equal number of nuclei are in an "up" (often called parallel) or "down" (also antiparallel) alignment. The minute difference between the two states creates a net magnetic moment. A measurable signal is generated from the magnetic moment after excitation by a radiofrequency (RF) pulse at the resonance Larmor frequency. This signal is generated as the excited nuclei in the body return to equilibrium, releasing energy in the form of an electromagnetic field that is captured by a receiver coil (Taouli et al, 2010).

The most common form of MRI is named structural magnetic resonance imaging (sMRI) and it translates the local differences in water content into different shades of gray that serve to outline shapes and sizes of the brain's various sub-regions as well as other organs, when receiving the information from the protons (Seeman P. & Madras B., 2014). An MRI scanner (Fig. 5) delivers a specific radiofrequency that excites hydrogen atoms in water molecules, which return some of this energy in the form of a characteristic nuclear magnetic resonance signal. Not all protons

behave that way, but enough do such that the resulting computer-generated image constitutes a highly detailed map of the organs tissues and structures. Thus, this tool can be used to discover the presence of abnormal tissue through the changes in density or composition. Scientists examining an sMRI can readily distinguish between gray and white matter and other types of tissue by their different shading and contrast with surrounding areas - both normal, such as blood vessels, and abnormal, such as tumors.

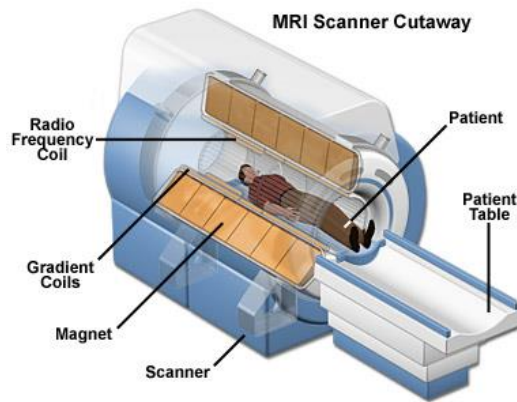


Figure 5. Magnetic resonance imaging machine scheme highlighting its components. (Source: nupex.eu/index.php?g=textcontent/nuclearapplications/nuclearinmed&lang=es)

Current diagnostic MRI scanners use superconducting magnets in the range of 0.5 Tesla (T) to 1.5 or even 3T. For comparison, the Earth's magnetic field is about 0.5 Gauss (G), that is approximately 0.00005 T. Cooling the magnet to a temperature close to absolute zero (0 K) allows such huge currents to be conducted, which is commonly achieved via immersion in liquid helium. Until recently, most clinical research was conducted at a field strength of 1.5 T. However, 3T systems are now widely available and are being used regularly as capabilities of 3T systems are being explored and optimized. The advantages of higher field strength systems include improved signal-to-noise ratio (SNR) (thus being able to lose less information) higher spectral, spatial, and temporal resolution, and improved quantification. Inherent disadvantages include magnetic susceptibility, eddy current artifacts, and magnetic field instability (Grover V. et al., 2015). The scanners are composed of two coils, the transmitter coils and receiver ones, and these may be either separate or coupled pieces of hardware, varying on the area of the body under examination. The applied RF pulse is emitted by an enveloping the transmitter coil, which

uniformly surrounds the area of interest, and the receiver coil consists of a loop of wire, which may either be placed directly over the region of interest or combined within the transmitter coil. Localizing the MR signal spatially to a region of interest requires the use of gradients. These are additional spatially linear variations in the static field strength. Gradients can be applied in any orthogonal direction using the three sets of gradient coils, G_x , G_y , and G_z , within the MR system.

T1 image contrast

Following the radio frequency (RF) pulse, transverse magnetization returns towards the longitudinal plane (axis of B_0) over a period of time known as the T1 relaxation time. This period is also known as the spin-lattice or longitudinal relaxation time. T1 differs between tissues, the extent of such differences depending upon a choice of image acquisition parameters, leading to image contrast. Clinically, T1 images provide good grey-white matter contrast and therefore anatomical information.

T2 image contrast

Tilting M (measurable signals) results in a rotational component in the xy plane, which is called an echo. Initially, all the proton axes are essentially rotating together (in phase) but begin to rotate at different speeds (dephasing), resulting in a loss of transverse M and therefore signal over a period termed T2 or the 'transverse magnetization time. This period is also known as the spin-spin relaxation time. The interval between the creation of transverse magnetization and its measurement is the echo time (TE). Only some tissues exhibit differences in T2, but an optimal TE exists for those and provides the best image contrast. T2-weighted images are particularly useful for imaging pathological processes in the brain, including white matter hyperintensities, demyelination, infarction and hemorrhage. Comparisons of these two types of images are presented in Figure 6 below.

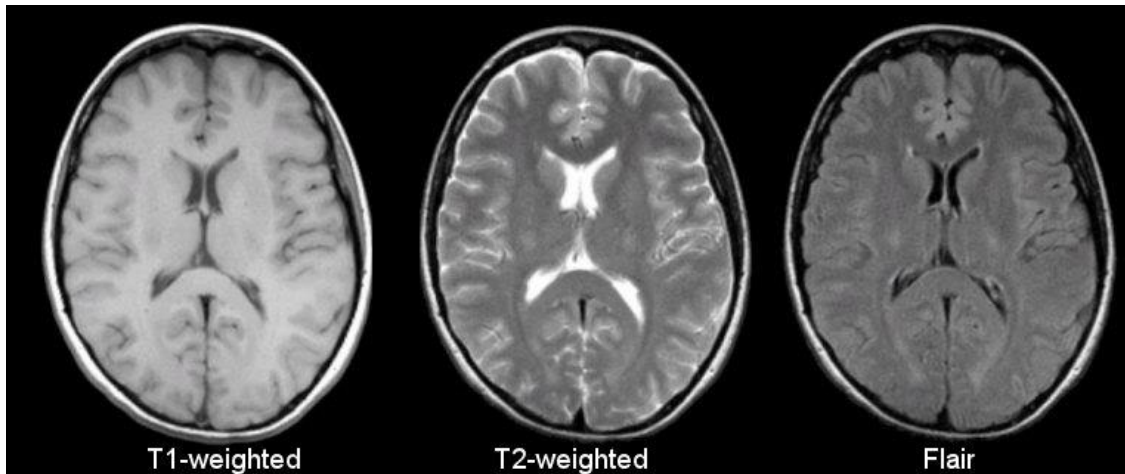


Figure 6. Comparison between T1, T2 and flair MRI results.
(Source: casemed.case.edu/clerkships/neurology/Web%20Neurorad/MRI%20Basics.html)

Although safe for the majority, there are some disadvantages while applying this technique, namely the claustrophobic feeling patients get while submitted to the exams, the prohibitive character of internal metallic hardware (like cerebral clips, pacemakers and such), physiological constrains like the glomerular filtration rate below 30 ml/min per 1.73m² due to risks associated to nephrogenic systemic fibrosis (NSF) while administrating intravenous common contrast agents like gadolinium, which has been demonstrated to deposit within soft tissues and organs, and even accumulating in the brain, when in free form (Wymer, 2010; Gulani, 2017).

There are major technologic advances in each of these modalities with the rapid changes in computer-based data manipulation. Three dimensional and even four-dimensional (time sensitive) image analysis are now available. “Molecular” imaging, in which biomarkers are used to visualize cellular function, is beginning to provide functional as well as anatomic information (Wymer, 2010).

1.3.2 Contrast substances and their importance

Contrast materials, also called contrast agents or contrast media, are used to improve imaging inside the body of patients in exams like X-rays, computed tomography (CT), magnetic resonance (MR) imaging, and ultrasound. Contrast materials are not dyes that permanently discolor internal organs but substances that temporarily change the way X-rays or other imaging tools the cells

and tissue. When introduced into the patient prior to an exam, these materials make certain structures or tissues in the body appear different on the images, than they would if no contrast material had been administered (as the presence of the contrast agent alters the relaxation characteristics of adjacent protons, thus indirectly affecting the intensity). They help distinguish (by means of contrast) selected areas of the body from surrounding tissue and by improving the visibility of specific organs, blood vessels or tissues, contrast materials help diagnose medical conditions, allowing the technician to distinguish normal from abnormal conditions (Wymer, 2010).

Administered doses of these agents enter the body in one of three ways, as they can be swallowed (taken orally) administered by enema (given rectally) or injected into a blood vessel (intravenously or intra-arterially). Following an imaging exam with contrast material, the material is absorbed by the body or eliminated through urine, usually within six hours about of 83% is eliminated (Zuckerberg, M. 2016). They can have a chemical structure that includes iodine, a naturally occurring chemical element (often injected and called positive agent, as the ones who follows) while others are barium-sulfate based (that is more commonly taken orally). Saline solutions (salt water) and gas (often air and called negative agents) are also used as contrast materials in imaging exams (Zuckerberg, M. 2016). Gaseous contrast agents absorb less amounts of X-rays than tissues due to their low density, while on the other hand, positive contrast agents absorb more x-rays than tissues because of their high density. In this specific case, gadolinium is the key component of the contrast material most often used in magnetic resonance imaging (MRI) exams. When this substance is present in the body, it alters the magnetic properties of nearby water molecules, which enhances the quality of magnetic resonance images. Although very common, gadolinium by himself is highly toxic, and is administered only when is firmly chelated (per example Gd-DTPA) (Wymer, 2010).

Although generally safe, minor reactions can occur in 3% to 5% of patients, some of the more common are mucosal reactions, urticaria, vomiting, local warmth and pain, headache, dizziness, among others (Committee & Contrastmedia, 2018). Severe life-threatening reactions and nephrotoxic reactions are rare, although it is not advisable for patients with renal insufficiency to take

gadolinium-based agents, as it presents some degree of nephrotoxicity (much less than iodinated ones) (Committee & Contrastmedia, 2018).

In respect to MRI its inherent drawback is its low sensitivity, as millimolar concentrations of protons are needed, and so the technique often requires use of exogenous contrast agents, like the ones mentioned above (Busquets, M. et al., 2015). These agents can alter relaxation processes (mentioned previously) when used in small amounts (of the order of nmol/L to $\mu\text{mol/L}$ concentrations). MRI contrast agents can broadly be divided into two classes: those that increase the T1 signal in T1-weighted images (positive contrast agent presenting bright contrast), and those that reduce the T2 signal in T2-weighted images (negative contrast agent, presenting dark contrast) (Busquets, M. et al., 2015). The effectiveness of a particular agent is defined by its longitudinal (r_1) and transverse (r_2) relaxivities rates.

Several NP-based contrast agents have been developed to overcome issues associated with conventional contrast agents – and successful improvements in chemical and photostability of NP fluorophores, and contrast agent detection limits, have been demonstrated in a broad array of imaging modalities (Kim, J. et al., 2017). The ideal NP based agent must fulfill a number of strict requirements: it should be easily dispersible and stable (resisting aggregation) in a variety of local *in vivo* environments and not be afflicted by differences in solvent polarity, ionic strength, pH, or temperature. It should exhibit limited nonspecific binding, be resistant to reticuloendothelial system (RES) uptake and it should have high sensitivity and selectivity for the target (like antigens, cells, tissues) with good contrast quality (high signal-to-noise ratio) and sufficiently long circulation times in the blood when administered intravenously (Kim, J. et al., 2017).

Current challenges and opportunities

One obstacle to be overcome when using NPs in these terms is the lack of reproducibility in its synthesis and in the functionalization to turn it biologically active. Batch to batch variations within the same laboratory, between laboratories, and even between different techniques employed in synthetic and modification procedures are common, often yielding the same NPs but with slightly different characteristics (per example purity of size distribution, number and type of conjugated biomolecules, stability, others). There is a need for consistency and scale-up in NP production

and functionalization, especially to produce high yields at low cost to permit commercialization and common use of these materials. As mentioned previously, the biggest knowledge gap existing in this research area is the lack of comprehensive characterization of NPs that are subsequently used in biological research and bioimaging. An in-depth understanding of the structure activity relationship of NP behavior in biological systems is imperative if researchers want to achieve better contrast agents - knowing what properties affect behavior will lead to more advances and improvements in this field. There are other implications on the fact that different bioimaging techniques require different and proper administered doses, based on the technique's sensitivity, host physiology, route of delivery, and the targeting strategy used (Hahn, 2010).

1.3.4 Iron nanoparticles in hyperthermia and MRI

Iron nanoparticles have been widely developed and produced for medical applications (e.g. diagnostic to achieve tissue contrast, cell labeling, drug delivery) (Bonder & Wang, 2009). Iron selenide (Fe_3Se_4) NPs, have been used as a thermal controller for hyperthermia treatments (Bonder & Wang, 2009). However, recent studies have also developed suspensions with iron oxide NPs for administration in patients. A German company named MagForce® AG carried out clinical tests with a formulation of Fe_3O_4 NPs coated with aminosilane, sizing 12nm, where approximately 5mL of the fluid was injected directly in patients' glioblastomas, which were then subjected to a bi-weekly treatment with 100kHz while receiving 30Gy of radiation therapy at 2Gy per fraction. This formulation presents great promises for hyperthermia technique application on deep tumors and has demonstrated a median overall survival of 13.4 months in glioblastoma patients, contrary to the typical median survival of about 6 months - so more than the double time, while exhibiting minimal toxicity. Iron oxide NPs have also been studied and developed for its use in radiological and MRI exams, as they are mainly superparamagnetic (Stephen, Z. et al., 2012). There are several types of iron oxide NPs, namely maghemite ($\gamma\text{-Fe}_2\text{O}_3$) magnetite (Fe_3O_4) and haematite ($\alpha\text{-Fe}_2\text{O}_3$) among which magnetite, is very promising, because of its proven biocompatibility. For molecular imaging purposes, the superparamagnetic iron oxide NPs (SPIONS) need to be biocompatible, non-toxic and magnetic. They also need to bind to a range of drugs, proteins, enzymes, antibodies, or other molecular targets. The iron oxide NPs can be

coated with a surface layer, usually of organic material, that provides an interface between the core and the surrounding environment. This surface layer can be used to direct the particles to a biological target site (Ruiz, 2015).

Iron oxide (Fe_3O_4) NPs are commonly coupled with a gadolinium (Gd) based metal-organic complex, in order to attain higher contrast between healthy and unhealthy tissues (Stephen, Z. et al., 2012). The most popular *in vivo* studied material for T2 contrast agents are these iron oxide NPs, which are generally coated with dextran, PEG, or other polymers, and their safety and effectiveness are influenced by their bio distribution and clearance of the organism. Based on their size, these NPs are classified as magnetic iron oxide nanoparticles (MION, μm), superparamagnetic iron oxide (SPIO, hundreds of nm), and ultra-small paramagnetic iron oxide (USPIO, <50 nm) (Stephen et al., 2012). The efficiency of iron oxide probes is size-dependent and increases with higher particle crystallinity.

When in aqueous media, these NPs may show some instability, which may impair their function. To increase the stability of NPs, they may be functionalized with molecules that bind to their surface. The two most common organic molecules that are used to functionalize this type of iron NPs is dopamine and its precursor, levodopamine. The use of dopamine and levadopamine as coating molecules is advantageous because both are naturally produced by biological systems, which enhance their adsorption during biomedical procedures (as they exhibit high affinity for biological membranes) and they are also expected to present low toxicity to humans and are easily degradable and expelled.

Dopamine (Fig. 7) is a member of small neurotransmitter molecules belonging not only to the central nervous system (CNS) but also to the periphery, and it is synthesized from the hydroxylation of the amino acid L-tyrosine (through tyrosine hydroxylase) into L-dopamine, which is then decarboxylated (through aromatic-L-amino-acid decarboxylase) to form dopamine (Syslova K. et al., 2012). It regulates neuroendocrine functions, locomotor activity, cognition and emotion. This neurotransmitter plays a prominent role in a variety of vital brain functions including motor control, short-term memory, attention and reward (Goldman-Rakic, 1998; Solanto, 2002). Its imbalances have been associated with stress-induced alterations in brain function and drug dependence, leading to diseases like in Parkinson's, schizophrenia, Gilles de la

Tourette's syndrome, Huntington's disease, depression, among others. The molecular actions of dopamine are mediated by five distinct receptor subtypes, some of which exist in different protein isoforms that can be attributed to alternative RNA splicing processes (Neve et al., 2004). Besides being the most studied neurotransmitter, it is also a highly conserved one and is found in numerous phyla, including worms, fruit flies, and snails (Carvey, 2010).

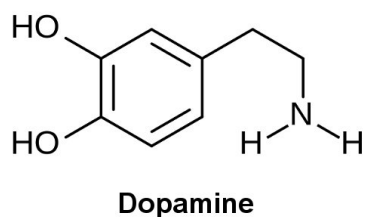


Figure 7. Structure of the dopamine molecule. (Source: wikipedia.org/wiki/Dopamine#/media/File:Dopamine.svg)

Levodopamine (L-DOPA) (or 3,4-dihydroxyphenyl-L-alanine) (Fig. 8) is an amino acid analog of L-tyrosine, present in the human body. Since the 1960s, L-dopamine has been used as a drug for Parkinson's disease, which is a degenerative disorder of the CNS and is usually caused by deficiency in the levels of the neurotransmitter dopamine in the brain. Because L-dopamine is a precursor of dopamine and can cross the blood-brain barrier (whereas dopamine itself cannot) it is possible to increase the dopamine level for the treatment of Parkinson's disease when the first one is administrated (Min, 2014).

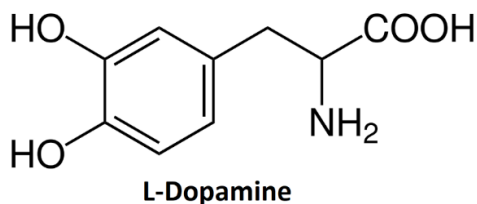


Figure 8. Structure of the levodopamine molecule. (Source: [wikipedia.org/wiki/L-DOPA#/media/File:3,4-Dihydroxy-L-phenylalanin_\(Levodopa\).svg](https://wikipedia.org/wiki/L-DOPA#/media/File:3,4-Dihydroxy-L-phenylalanin_(Levodopa).svg))

The toxicity of these iron NPs, has been scarcely studied, namely those of iron selenide. Regarding iron oxide NPs, they have been found to accumulate in the liver, lungs, spleen and brain (evidencing their ability to cross the human BBB). *In vivo* studies on human cancerous cells lines

have shown that after entering the cells, these NPs remain in cell organelles (endosomes or lysosomes) being released into cytoplasm after decomposing and contributing to the cellular iron pool (Chen, J. et al., 2013). Evidence show that these NPs exert their toxic effect in the form of cell lysis, inflammation, and disturbing blood coagulation system. Reduced cell viability has also been reported as a common toxic effect in *in vitro* studies (Bahadar H. et al., 2016). Iron oxide NPs coated with different molecules have shown variable cell viability results – low concentrations (25-200 µg/mL) of these NPs coated with Tween (a surfactant) exhibited higher cell toxicity than higher concentrations (300-500 µg/mL) in murine macrophages as found by Naqvi et al. (2013), while in other studies on mouse neuroblastoma cell lines (Neuro-2A), the same NPs have been found to present less toxic effects in terms of cell apoptosis, morphology and permeability but also mitochondrial functions, when presented in concentrations from 10 µg/mL to higher than 200 µg/mL (Jeng and Swanson, 2006). In relation with iron selenide, there is still a lack of scientific knowledge on its toxicity, most published works only address their synthesis.

1.4 Objectives

The aim of the present study was to evaluate the influence of chemical composition and coating in the toxicity of iron superparamagnetic nanoparticles (NPs) to freshwater biota. For this, two iron NPs coated with dopamine were selected to be studied: iron(II) selenide ($\text{Fe}_3\text{Se}_4@Dopa$) and iron(III) oxide ($\text{Fe}_3\text{O}_4@Dopa$). To evaluate the influence of coating in the toxicity of the NPs, Fe_3Se_4 were also produced with levadopamine as a coating agent ($\text{Fe}_3\text{Se}_4@Dopa$).

2. Materials and Methods

2.1. Nanoparticles studied

Two metallic nanoparticles (NPs) were selected to perform the present study: iron selenide (coated with dopamine- $\text{Fe}_3\text{Se}_4@Dopa$ and levadopamine) and iron oxide (coated with dopamine- $\text{Fe}_3\text{O}_4@Dopa$). Their general dimensions consist in a range from 56 to 350 nm for Fe_3Se_4 and from 16 to 24 nm for Fe_3O_4 . Their shape usually resembles a sphere in its core with a layer of the

coating covering it. These NPs were synthesized at the Department of Chemistry and Aveiro Institute of Materials, both from the University of Aveiro, by MSc Rute Pereira.

2.1.1 Nanoparticles synthesis process

The size-controlled synthesis process of the NPs involved the biochemical protocols described below. The main advantages of this synthesis includes low cost, environmental friendliness (produces less residues than current synthesis processes) and it is highly resistant to corrosion (Zhao et al., 2014). One key factor for determining the particles' physicochemical properties are their synthesis conditions, which can alter concentrations, pH of the solution where they are suspended, and others (Mamani et al., 2014).

The particles were later characterized through TEM (transmission electron microscopy), XRD (X-ray diffraction), and zeta potential techniques, regarding its physical properties as size, structure, and stability.

Fe₃O₄ Nanoparticles

The synthesis of Fe₃O₄ NPs was adapted from Guardia et al. (2011). In a round bottom flask, 0.7190 g of Fe(acac) (III) and 2.332 g of decanoic acid were mixed in 50 mL of dibenzyl ether. The mixture was purged in vacuum during 1 hour at 20 °C, and then placed under a Nitrogen atmosphere. The mixture was then heated until 200 °C for 2 hours, with an heating rate of 6 °C/minute. The temperature was later increased until reflux was observed (around 275 °C) for 1 hour, and then cooled until room temperature. The NPs were collected through centrifugation (30 min at 3.52G) and washed with a mixture of ethanol/hexane (2:1). The NPs were later dried and collected for storage.

Fe₃Se₄ Nanoparticles

Se-ODC (selenium-octadecene) is a metal-organic complex that is needed before synthesizing Fe₃Se₄ NPs, and it was chosen because of its reactivity and stability. This synthesis was adapted from the protocol used by Bullen et al. (2010). In a round bottom flask, 283 mg of selenium powder were dissolved in 154 g of octadecene. The mixture was purged under vacuum at 120 °C. After 1 hour, the mixture was then placed under a nitrogen atmosphere and the temperature

was increased to 215 °C. After 10 minutes the reaction was cooled to room temperature and reserved in a flask for further usage. Afterwards, in a round bottom flask, 58.5 mg of Fe(acac) (III), 10.2809 g of Se-ODC, 15.3 mg of 1-dodecanethiol (DDT) and 23.7 mg of tetradecylphosphonic acid (TDPA) were mixed and purged in vacuum at 70 °C. After 1 hour, the mixture was placed under a Nitrogen atmosphere and heated up to 250 °C during 30 minutes with a heating rate of 5 °C/minute. The reaction was then cooled until room temperature and the nanoparticles were washed with hexane, collect through centrifugation (15 min at 3.52G) and dried for storage.

2.1.2 One-step phase exchange and functionalization

The two types of NPs were dispersed in ethanol with the help of an ultrasonic bath. Then, the coating agent (dopamine or levodopamine) was added, and the mixture was left stirring under Nitrogen at 50 °C for 3 hours. The resulting mixture was then cooled and collected. The functionalized NPs were collected, washed 2 times with ethanol, and then dried in a fume hood. After adding 2 mL of water and leaving a few minutes dispersing inside an ultrasonic bath, the particles appeared to be stable in water.

The quantities of NPs, surface agent and ethanol varied as follows:

- A dopamine functionalization was achieved mixing 10 mg of NPs, 50 mg of dopamine hydrochloride and 10 mL of ethanol.
- A levodopamine functionalization included 10 mg of NPs, 60 mg of levodopa and 10 mL of ethanol.

2.2 Model species

To evaluate the potential toxicity of the selected NPs, species belonging to different trophic levels (producers, primary and secondary consumers) were selected. The selected species are well and extensively described being recommended for toxicity assaying by several guidelines (e.g., OECD 201, 2006; OECD 221, 2006; Hymne et al. 1996; MicroBiotests, Gent, Belgium).

2.2.1 Producers organisms

Microalgae can grow in both fresh and marine water as well as in almost every environmental condition on earth ranging from high to low temperatures/altitudes and they present an enormous biodiversity from which about 40.000 species are already described (Safi, 2014). They

are key species that provide oxygen and intervene in freshwater nutrient cycling. Alongside, they are a very important part of the food chain, being a direct food source for higher trophic levels (e.g., zooplankton) that are afterwards consumed by other invertebrates, fishes or even birds. For this reason, results of toxicity tests with algae are part of the basic information required for the evaluation of environmental hazard of chemicals as recommended internationally by the Organization for Economic Cooperation and Development (OECD 201, 2006) and demanded in many other legislations acts, as REACH (European Union) (Gustavsson, 2017) and Rotterdam Convention (2004) (Suzuki, 2018). A number of studies have found algae to be more sensitive than fish not only to chemicals (general ones, active pharmaceutical ingredients, metals, others) but also for synthetic nanoparticles (Hutchinson *et al.*, 2003). The microalga *Raphidocelis subcapitata* was selected in the present work to run toxicity assays. It presents a curved appearance with a crescent heliptical shape, it is planktonic and normally occurs in a solitary form (Fig. 9). It has a length between 6 and 14 μm , and a width between 2 and 3 μm and are usually involved by a colourless mucilage (Aruoja, 2011).

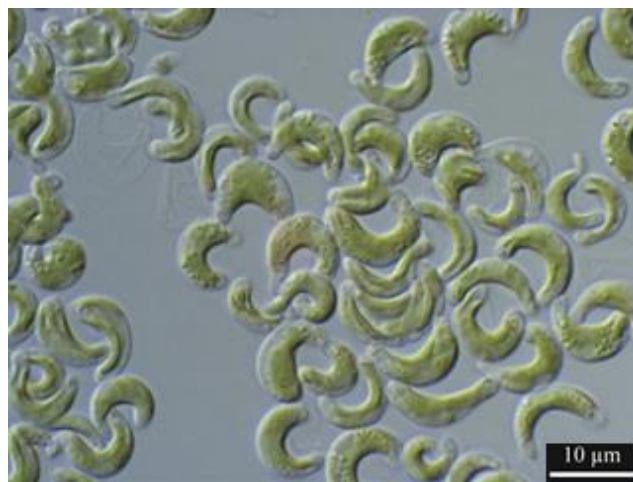


Figure 9. Images showing cells of the microalga *Raphidocelis subcapitata*.
(Source:shigen.nig.ac.jp/algae/images/strainsimage/nies-0035.jpg)

The microalgae culture was maintained in 250mL sterilized erlenmeyers flasks containing MBL medium (annex 1) under continuous light at an intensity of $100 \mu\text{E m}^{-2} \text{s}^{-1}$ and temperature at 23°C , accordingly to OECD guideline 201 (OECD, 2006). Cultures were renewed once a week.

Macrophytes

Along with the microalgae, also the macrophytes are commonly employed as model species in preliminary risk assessment frameworks because it presents high sensitivity to organic and inorganic compounds, is easy to handle, being often used as research organisms for studies in areas such as physiology, genetics, ecology, environmental monitoring, ecotoxicology (Scheer, 2007). The common duckweed (*Lemna minor*) (Fig. 10) is a free-floating small monocotyledonous freshwater macrophyte of Lemnaceae family (Scheer, 2007). It has also a cosmopolitan distribution, spreading rapidly in stagnant or slow-moving fresh water, from mesotrophic to eutrophic ecosystems and tolerating a wide range of pH values. It's fronds are often used by other organisms as a refuge.

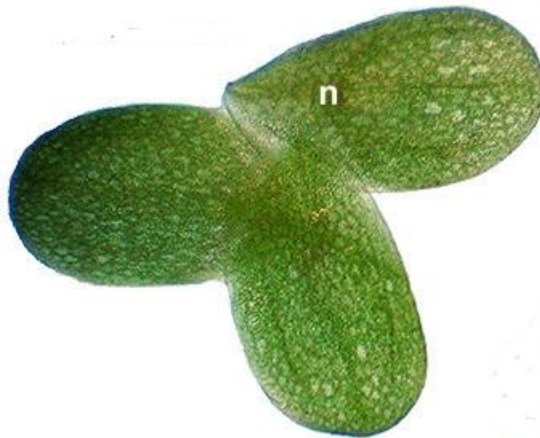


Figure 10. Image of *Lemna minor* with three fronds (n). (Source: palomar.edu/users/warmstrong/imglemi.htm)

The cultures of the macrophyte *L. minor* were maintained in 250 mL sterilized glass vessels with Steinberg medium (annex 2) under controlled conditions of light (continuous white-fluorescent at an intensity of $100 \mu\text{E m}^{-2} \text{s}^{-1}$) and temperature (23°C), following OECD guideline 221 (OCED, 2006b). Culture medium was renewed twice a week.

2.2.2 Consumers organisms

Rotifers

Rotifers are freshwater planktonic multicellular organisms that generally measure less than 1 mm but their length can range from about 40 μm to 2 mm (O'Reilly, M., 2001) and belong to the Phylum Rotifera. These organisms are considered broadly cosmopolitan and can be found in diverse environments. The body of rotifers is constituted by several cavities that are covered by the mesoderm and specialized organ systems with a complete digestive tract including both a mouth and anus (Segers, H. 2007). Their diet is based on filter feeding and consists in organic matter or organisms small enough they can ingest, like protozoans and principally microalgae. They reproduce mainly by parthenogenesis; some species produce females from unfertilized eggs, while others tend to produce two types of eggs with distinct sexuality, but males hatching from these eggs are not able to survive since they are not capable of feeding (Segeer, H. 2007). In addition to this, their short and quick life cycle and their sensitivity to chemicals makes them a good model species for ecotoxicological studies. In the present work the rotifer species *Brachionus calyciflorus* was selected to run toxicity assay (Fig. 11). Cysts of rotifers were obtained from hatching Rotoxkit F kits (MicroBioTests, Gent, Belgium).



Figure 11. Image of *Brachionus calyciflorus*. (Source: <https://alchetron.com/Brachionus-calyciflorus#demo>)

Hydra

Hydra is one of the few genera of the phylum Cnidaria, class Hydrozoa (among other six classes) that has adapted to freshwater and appears as really simple organisms with radial symmetry as their tubular body (up to 10mm) is constituted by a simple pair of two cell layers (so denominated diploblastic organisms) separated by a thin gelatinous non-cellular extra layer, the mesoglea (Bouillon, et al., 2006). The outer cell layer is called ectoderm, which originates the nematocysts and the inner one is called endoderm, which segregates enzymes that participate in the digestion process (Bouillon et al., 2006). Each tentacle, or *cnida* is coated with highly specialized stinging cells named cnidocytes that contain structures called nematocysts. Upon contact with prey, the contents of the nematocyst are discharged, liberating neurotoxins into other organisms (Folino, 2015).

This class is also the most abundant, widespread and better studied of the phylum Cnidaria (Campbel, 2016). This group is represented by more than 10,000 species in aquatic habitats around the world in which fewer than 40 species occur in freshwater habitats (Folino, 2015). They can be found in any unpolluted freshwater matrix like ponds, lakes, and streams in the temperate and tropical regions – this genus is known to have a cosmopolitan distribution (Folino, 2015). Their nervous system is structured like a net that connects sensory photoreceptors and touch sensitive cells located in the body walls and tentacles of the organisms. They lack specialized internal organs for excretion, circulation and respiration, so diffusion of metabolic wastes and gases occurs at the cellular level throughout the epidermis. For the excretion of the indigestible remains of food items, hydras contract their entire bodies and expel them through the mouth aperture, after two or three days of capturing it. Hydra are able to expand its body walls so that one may digest preys which are more than twice their size (Thorp, 2011).

Most of the Hydrozoa species go through metamorphosis, changing from a free-floating polyp (sessile) to and adult form (motile) called medusa, this does not occur in the Genus *Hydra*, these organisms remain as polyps their entire lives. Most freshwater Cnidaria are primarily carnivores. *Hydra viridissima* (Fig. 12) not only passively preys but also obtains nutrients from an endosymbiotic relationship with algae of the Genus *Chlorella* (Folino, 2015). Their prey usually

consists in small crustaceans, worms, mosquitoes and other insect larvae, and occasionally small larval fish. The main predators of hydras are fishes, flatworms, crayfishes, amoebas and other types of predators. Hydra may sexually produce eggs or have offspring that bud off asexually from the parent, asexual budding occurs more frequently than sexual reproduction (Thorp, 2011).



Figure 12. Image of *Hydra viridissima* with sprout (attached to a substrate). (Source: http://www.hlasek.com/hydra_viridissima_bt5106.html)

The genus hydra has been extensively cultured and studied by biologists in almost every biological field going from molecular physiology to ecotoxicology (Folino, 2015). Hydras were cultured in Hydra medium (annex 4) in round glass vessels at 20°C. Culture medium change and feeding (with nauplii of *Artemia salina*) occurred twice per week.

Amphibians

The species of amphibian most widely used in scientific research are *Xenopus tropicalis* (Tropical clawed frog) and *X. laevis* (African claw-toed frog), from Family Pipidae. They are autochthonous in the African continent, occurring in Angola, Camerouns, Congo, Zambia, among others. *Xenopus laevis* is considered an invasive species in some countries in Europe, like France and United Kingdom, and also in the United States of America (Fig. 13) (Tinsley, R. et al., 2009). It is completely water dependent, breeds in water matrices, preferably in shallow waters without a strong flow and occurs both in reference ponds and in anthropogenic impacted environments,

evidencing high adaptation to environmental degradation. It lives in all kinds of waterbodies, except larger ones, and it has a high opportunistic sense, having high mobility and endurance, easily colonizing new environments or newly created habitats (Tinsley, R. et al., 2009).



Figure 13. Image of *Xenopus laevis*, male in the left and female in the right. (Source: Shuji Takahashi, Hiroshima University, 2016).

This species is commonly used in scientific research due to its biological and ecological particularities which confers them advantages over other *taxa* namely, they lay hundreds of transparent eggs, are easily breed and maintained in laboratory conditions, having bare skin as well as benefiting from great knowledge by the scientific community, on its biology/ecology and evolutionary similarities with humans. Another main advantages of using *X. laevis* organisms is the fact that not many amphibian species react to human chorionic gonadotropin to induce amplexus and egg release (Mann, Hyne, & Choung, 2010).

Handling and maintenance

Organisms are maintained in glass aquariums (Fig. 14) with lids (to prevent escaping) and a water column with 6 to 6.5 cm of height, on average. The room temperature is kept at 23 °C with a photoperiod of 16:8 hours light:dark. Each aquarium holds one adult organism.



Figure 14. Image of a *Xenopus laevis* holding aquarium. (Source: Pedro Nunes, 2018)

Adults are fed 4 to 5 mealworms (*Tenebrio molitor* larvae) (Fig. 15) and 2 to 3 proper pellets three times a week. Aquariums are siphoned, their debris and waste withdrawn, and water replaced twice a week and totally cleaned one a week.



Figure 15. Image of the pellets (left) and wholeworms (*T. molitor*) (right) used to feed *Xenopus laevis*. (Source: Pedro Nunes, 2018)

Tadpoles are kept and maintained in the same room conditions as the adults, but in large quadrangular plastic recipients in FETAX medium (annex 5), until used in any assay. They are fed with common fish food (TetraMin™ from Tetra™) every other day, and their containers cleaned, where occurs the medium change.

Reproduction and egg harvesting

Eggs were obtained by inducing amplexus via injection of the commercial human chorionic gonadotropin (500 units for the female and 150 units for the male; HCG was obtained from Sigma®; (Fig. 16) in the dorsal lymph sac (Fig. 17).

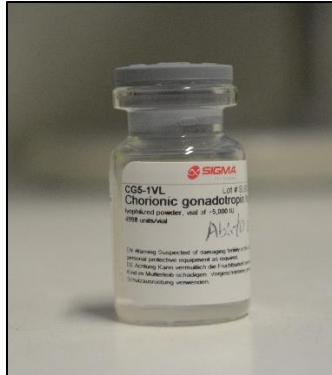


Figure 16. Human chorionic gonadotropin hormone vial flask. (Source: Pedro Nunes, 2018)

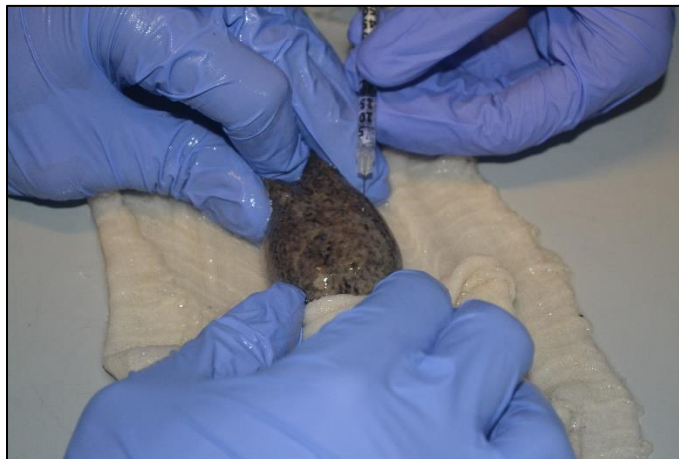


Figure 17. Image of *Xenopus laevis* being injected with human chorionic gonadotropin. (Source: Pedro Nunes, 2018)

After reproduction, eggs are collected and put into FETAX medium, without the removal of the biological protector jelly, as it is desirable to keep the study as much ecologically relevant as possible, mimicking natural conditions.

2.3 Toxicological assays

2.3.1 Toxicological assays with producers

Microalgae

The 72-h assays with microalgae (*R. subcapitata*) followed the OECD guideline 201 (OECD, 2006) adapted for 24 well plates after Moreira-Santos et al. (2004). Firstly, at the beginning of the assays, an initial concentration of cells (10^4 cells ml^{-1}) was prepared recurring to a Neubauer counting chamber (Fig. 18). The microalgae were exposed to a control (MBL medium) and 6 tested concentrations for each NP (ranging from 75.7 to 197 mg/L). Three replicates, each with 1mL of test solution, were performed for each treatment. The test plates were kept at a controlled temperature of 23°C and continuous light conditions ($100 \mu\text{E m}^{-2} \text{s}^{-1}$) during the 72h exposure period.

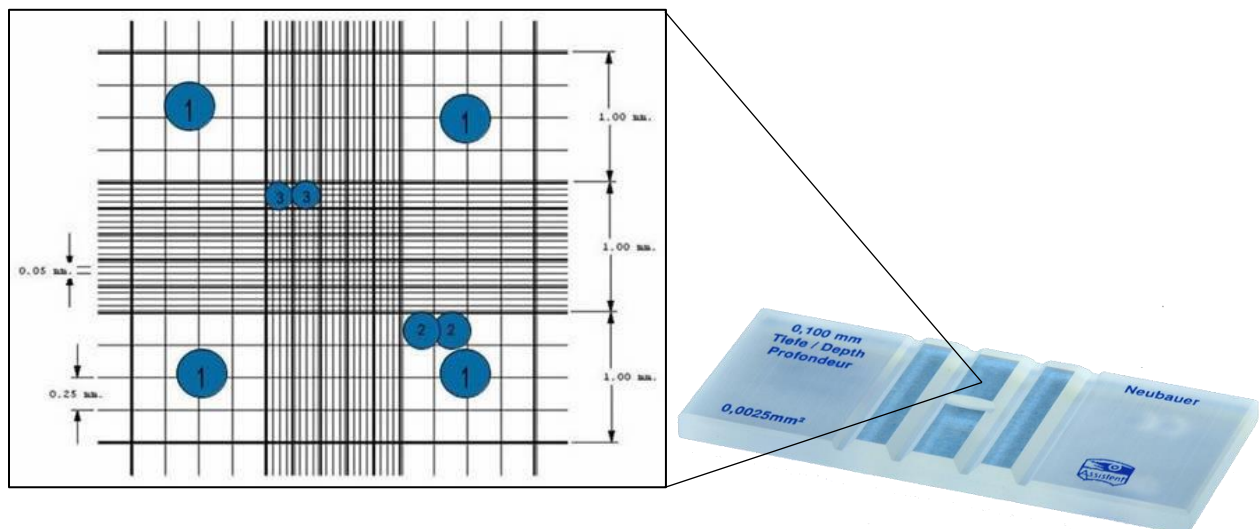


Figure 18. Neubauer chamber for cell counting illustration. (Source: laboratoryinfo.com/manual-cell-counting-neubauer-chamber/)

At the beginning and end of the assay, algal growth was accessed by measuring the absorbance (ABS) at 440 nm through Jenway 6505 UV/VIS spectrophotometer (Burlington, VT, USA). Then, obtained values were converted into cell density (number of cells per ml) according to equation 1:

$$\text{Conc. (cell ml}^{-1}\text{)} = -17107.5 + (\text{ABS} * 7925350) (R^2 = 0.99), \text{ for } R. \text{ subcapitata (equation 1)}$$

Average specific growth rate (μ day⁻¹) was determined after OECD201 (2006) guideline for each tested concentration and control as follows:

$\mu_{i-j} = \frac{\ln X_j - \ln X_i}{t_j - t_i}$ (day⁻¹), where μ_{i-j} is the average specific growth rate from time i to j; X_i is the biomass at time i; X_j is the biomass at time j;

The percentage of specific growth rate inhibition relatively to the control was calculated after the previous guideline as follows:

$\%I_r = \frac{\mu_c - \mu_r}{\mu_c} \times 100$, where $\%I_r$ is the percent inhibition in average specific growth rate; μ_c the mean value for average specific growth rate (μ) in the control group; μ_r the average specific growth rate for the treatment replicate;

Macrophytes

The 7-day growth assays with the macrophyte species *Lemna minor* were performed following the OECD 221 guideline (OECD, 2006b), adapted to 6-well plates. At the beginning of the assays, three seedlings with the same number of fronds (in a total of 12) and no visible necrosis or defects were assigned per each well (Fig. 19). Each well was filled with 8mL of control medium (Steinberg: annex 2) or test concentrations (9 tested concentrations: 80-200 - for Fe₃Se₄@Dopa and Fe₃O₄@Dopa and other 9 tested concentrations: 16- 95 mg/L for Fe₃Se₄@L-Dopa. Three replicates were performed per treatment. Plates were incubated at 23°C with continuous light conditions (100 μ E m⁻² s⁻¹) for 7 days.



Figure 19. Image of *Lemna minor* assay plaque. (Source: Pedro Nunes, 2018)

At the end of the assay total number of fronds and the number of necrotic fronds were counted per well. The average growth rates were calculated (as $\mu \text{ day}^{-1}$) as follows:

$$\mu_{i-j} = \frac{\ln X_j - \ln X_i}{t_j - t_i} \text{ (day}^{-1}\text{)}, \text{ where } \mu_{i-j} \text{ is the average specific growth rate from time } i \text{ to } j;$$

X_i is the biomass at time i ; X_j is the biomass at time j ;

2.3.2. Toxicological assays with consumers

Rotifers

The 24-h mortality assay with the freshwater rotifer *B. calyciflorus* was performed following the standard procedures included in the Rotoxkit F kit (MicroBioTests, Gent, Belgium). Neonates of the rotifer *B. calyciflorus* were obtained after hatching of the cysts included in the previously acquired commercial kit RotoxKit F (MicroBioTests, Gent, Belgium) (Fig. 20). The hatching process was initiated 16-18 hours prior to the start of the assays adding 1.5 ml of proper cysts medium (annex 3) on a test plate, after emptying one cysts vial. Cysts were hatched at 23°C, for 24 hours, at a constant light intensity of 3000-4000 lux.



Figure 20. Rotoxkit F (MicrioBioTests, Gent, Belgium) hatching kit. (Source: <http://ambifirst.pt/produtos/microbiotests-toxkit/>)

Rotifers were exposed to seven concentrations (ranging from 17.6 to 200 mg/L) of each NP plus a negative control (Rotifer media; annex 3). Five replicates with five newly hatched rotifers per each concentration and control were carried out. After 24 hours of exposure, mortality was assessed through the analysis of motility of the organisms, considering dead an organism that did not show any movement within 5 seconds of observation after gentle agitation of the exposure medium. Exposure occurred at 23°C in the dark.

Hydras

A 96-h mortality and malformation assay was carried out with the freshwater cnidarian *H. viridissima*. This same assay was followed by a post-exposure 30-min feeding assay. The first one was done in 24 wells plates and it was tested a control with Hydra medium plus 8 concentrations (from 50 to 198 mg/L). It were evaluated endpoints like mortality and malformations, which were attributed score corresponding to each type of malformation, after Wilby et al. (1989) as seen on Fig. 21. The assays were kept at 20°C with a photoperiod of 16 hours of light ($100 \mu\text{E m}^{-2}\text{s}^{-1}$) and 8 hours of darkness.












										
Normal	Increasing Degree of Toxicity						Osmoregulation loss	Terminal States		
Extended tentacles and body, reactive.	Partially contracted slow reactions.	Clubbed tentacles. Body slightly contracted.	Shortened tentacles.	Tentacles and body shortened	Totally contracted tentacles visible.	Totally contracted no visible tentacles.	Expanded, tentacles visible.	Expanded, no visible tentacles.	Dead but intact.	Disintegrated
Score 10	Score 9	Score 8	Score 7	Score 6	Score 5	Score 4	Score 3	Score 2	Score 1	Score 0

Figure 21. Classification for *Hydra viridissima* morphological, on a scale of scores from 0 to 10. (Source: Wilby et al. 1989)

After the 96h exposure the feeding assay was carried out. The exposure medium was changed, and hydras were carefully washed with clean medium. After, each well was filled with 2 mL of clean medium (hydra medium; annex 4) to assess the feeding capacity. Each hydra was exposed individually and was allowed to fed for 30-min on 10 *Artemia salina* organisms. After that period, remaining organisms were counted, and it was calculated the feeding ratios of the surviving hydras.

Amphibians

Embryos at Gosner stage 10-11 (Gosner, 1960) were exposed to a control (FETAX) and to 5 concentrations of the NPs (ranging from 13.1 to 100 mg/L), by following the standard protocol of ASTM (1998). Four and two replicates were carried out for the control and each concentration of the NPs, respectively. Each replicate contained 10mL of the test solution and 25 embryos. Exposure took place at 23° C with a photoperiod of 16:8 hours light:dark. At the end of the assay the presence of malformations and mortality were monitored.

2.4 Statistical data treatment

Computation of the concentrations causing 20 and 50% of mortality (LC₂₀ and LC₅₀) were obtained by fitting data sets to a linear regression model (Probit analysis software). The effective concentrations (EC₂₀ and EC₅₀) were obtained after fitting data sets to a three-parameter log-logistic models in Statistica 8.0 software for Windows.

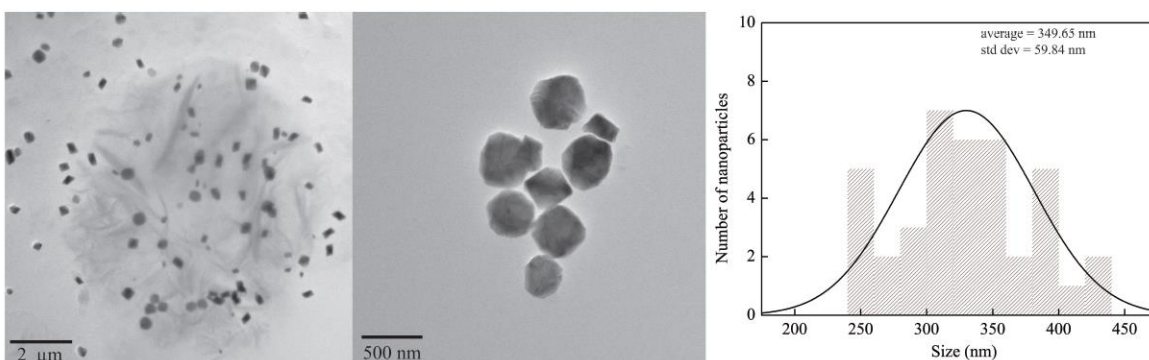
All data sets were checked for normality (Shapiro-Wilk test) and equality of variances (Levene's test). To check for significant differences between treatments and control conditions (for each species and endpoint, individually) it was employed a one-way ANOVA analysis followed by Dunnett's. Whenever the assumptions of the parametric ANOVA were not met the Kruskal-Wallis test was carried out followed by the Dunn's test. Statistical differences were considered whenever $p < 0.05$. Analyses were performed in SigmaPlot 12.5 software for Windows.

3. Results

3.1 Nanoparticles characterization

Measurements made with X-ray diffraction showed an average size of 56.1 nm for Fe_3Se_4 and 24 nm for Fe_3O_4 .

The images obtained with TEM revealed a good control in the shape of the two NPs (Fe_3Se_4 and of Fe_3O_4) (Fig. 22). Regarding size distribution, the NPs of Fe_3Se_4 exhibited a larger size distribution than that observed in Fe_3O_4 NPs. The former showed a size average of 350 nm (higher than the value obtained by X-ray diffraction) and the latter of 16.6 nm (slightly lower than the value obtained by X-ray diffraction).



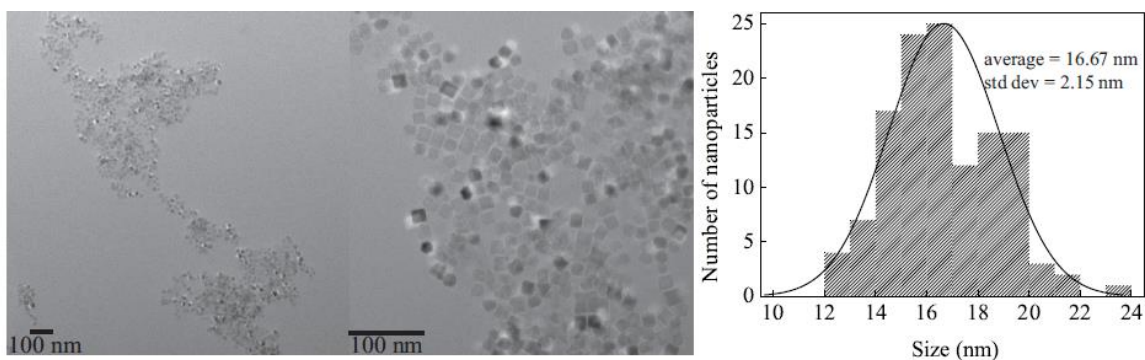


Figure 4. Transmission electron microscopy images and size distribution of Fe_3Se_4 (up) and Fe_3O_4 (down) nanoparticles (Source: Pereira, R., 2018).

The zeta potential of Fe_3Se_4 @Dopa, Fe_3Se_4 @Levodopa and Fe_3O_4 @Dopa were, respectively: +3, -20 and +32 mV, indicating a lower stability of Fe_3Se_4 @Dopa.

3.2 Ecotoxicity assays

A resume table of all the calculated ECs is present in annex 6.

Producers organisms

3-day growth inhibition assays with *Raphidocelis subcapitata*

Exposure to nanoparticles of Fe_3Se_4 @L-Dopa, Fe_3Se_4 @Dopa and Fe_3O_4 @Dopa induced no significant effects in the specific growth rate and yield of *R. subcapitata* relatively to the control (Fig. 23; Dunn's: $p \geq 0.125$). Nevertheless, though not being statistically significant, a decrease in specific growth rate and yield above 25% was registered at the four and three lowest tested concentrations of Fe_3Se_4 @Dopa and Fe_3O_4 @Dopa, respectively (Fig. 23).

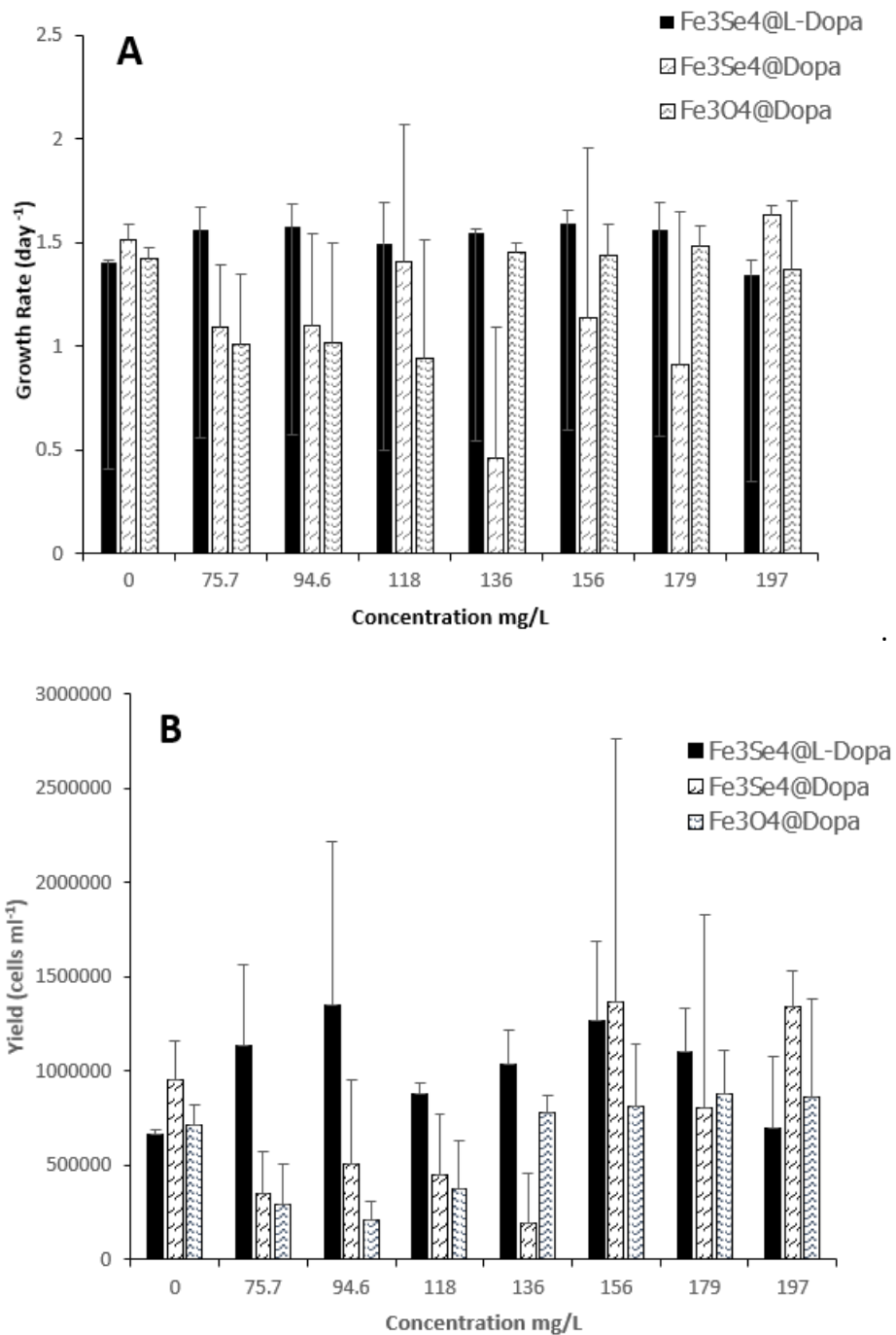


Figure 23. Average of specific growth rate (A) and of yield (B) of the green microalgae *Raphidocelis subcapitata* after a 3-day exposure period to three iron nanoparticles (iron selenide coated with Levodopamine – Fe₃Se₄@L-Dopa; iron oxide coated with Dopamine - Fe₃O₄@Dopa; and iron selenide coated with Dopamine – Fe₃Se₄@Dopa). Error bars correspond to the standard deviation.

7-day growth inhibition assays with *Lemna minor*

In the 7-day growth inhibition assays with the macrophyte *L. minor*, significant reductions (> 10%) were observed in the number of frond at all tested concentrations of Fe₃Se₄@L-Dopa (Fig. 24; Dunnett's: <0.001). The value of EC₅₀ computed for this nanoparticle was 23 mg/L (95% confidence limits-CL: 19.96-27.63) while for EC₂₀ it was not possible to calculate.

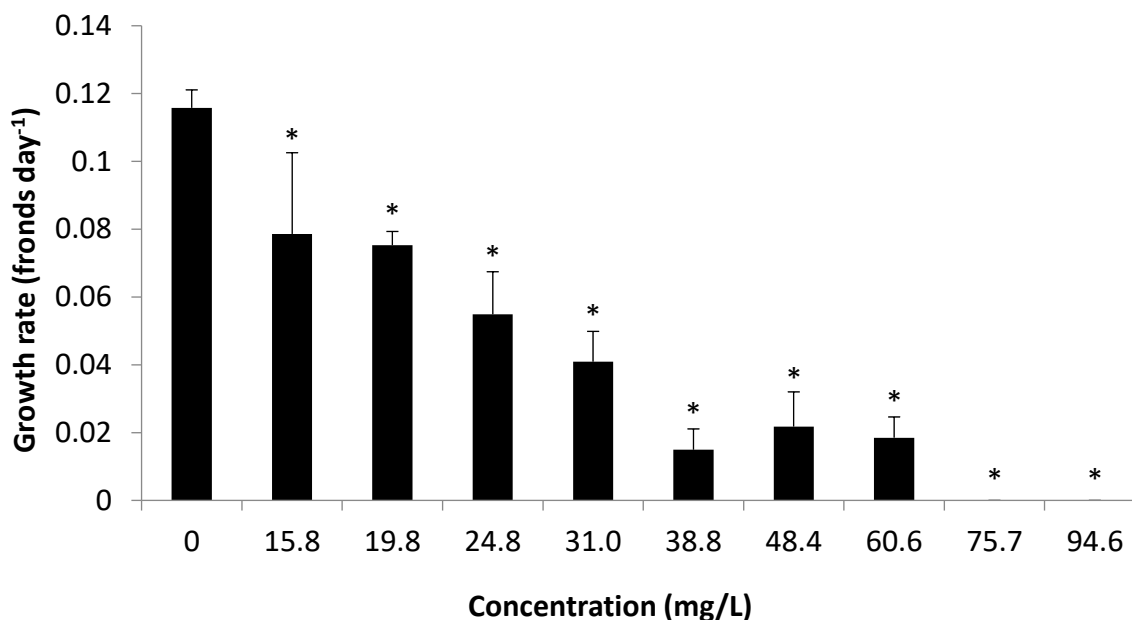


Figure 24. Average growth rate of *Lemna minor* fronds after a 7-day exposure period to nanoparticles of iron selenide coated with levodopamine (Fe₃Se₄@L-Dopa). Error bars correspond to the standard deviation. * indicates significant differences relatively to the control (Dunnett's, $p < 0.001$).

Exposure to nanoparticles coated with dopamine also caused significant reductions in the growth rate of *L. minor*, but at concentrations higher than the ones inducing effects by nanoparticles coated with levodopamine: for Fe₃Se₄@Dopa concentrations equal or above 166 mg/L and for Fe₃O₄@Dopa concentration 200mg/L (Fig. 25). The EC₂₀ and EC₅₀ computed for Fe₃Se₄@Dopa were 142. mg/L (95% CL: 1301-155) and 126 mg/L (95% CL: could not be computed), respectively. For Fe₃O₄@Dopa EC₅₀ obtained was 204 mg/L (95% CL: could not be computed) while EC₂₀ could not be computed.

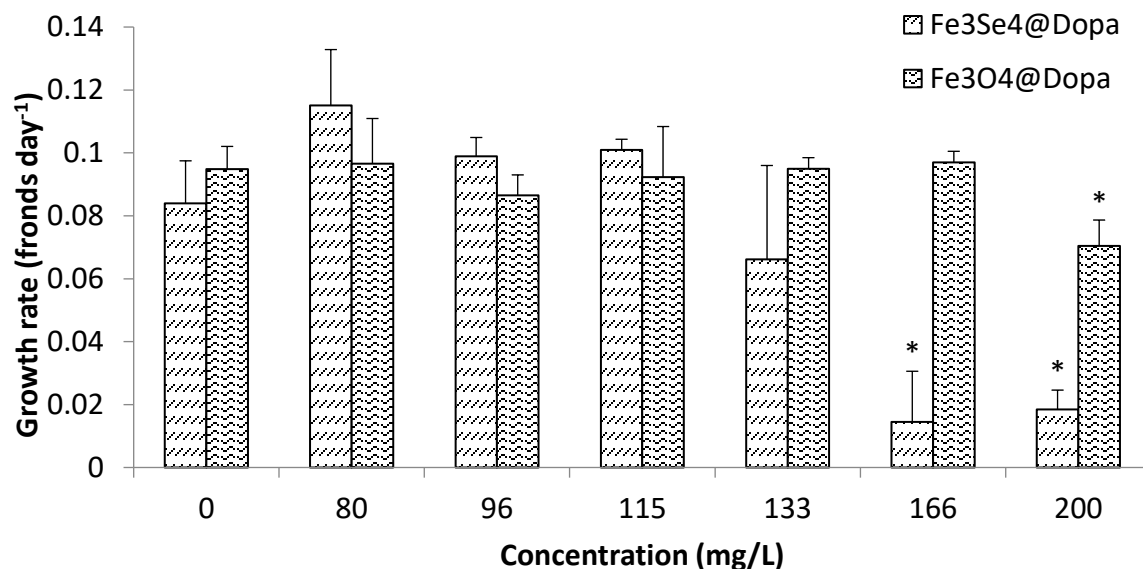


Figure 25. Average growth rate in *Lemna minor* fronds after a 7-day exposure period to two iron nanoparticles (iron oxide coated with Dopamine - Fe₃O₄@Dopa; and iron selenide coated with Dopamine - Fe₃Se₄@Dopa). Error bars correspond to the standard deviation. * indicates significant differences from the respective control (Dunnett's, $p < 0.05$).

Consumers

24-hours acute assay with *Brachionus calyciflorus*

Survival of the rotifer *B. calyciflorus* was significantly reduced after exposure to the three nanoparticles (Fig. 26). Mortality above 60% occurred in organisms exposed to concentrations equal or higher than 88.9 mg/L of Fe₃Se₄@Levadopa and equal or higher than 39.5 mg/L for Fe₃Se₄@Dopa (Fig. 26). Organisms exposed to Fe₃O₄@Dopa only showed significant mortality (68%) at the highest tested concentration (Fig. 26). Nevertheless, a mortality equal or above 20% was observed for all NPS at 17.6 mg/L (Fig. 26). The EC₂₀ and EC₅₀ were, respectively, as follows: 15.4 mg/L (95% CL: 6.22-23.0) and 50.6 mg/L (36.3-67.8) for Fe₃Se₄@Levadopa; 18.9 mg/L (13.2-24.3) and 10.4 mg/L (4.84-14.5) for Fe₃Se₄@Dopa; and 12.5 mg/L (0.004-30.6) and 240 mg/L (106-2687) for Fe₃O₄@Dopa.

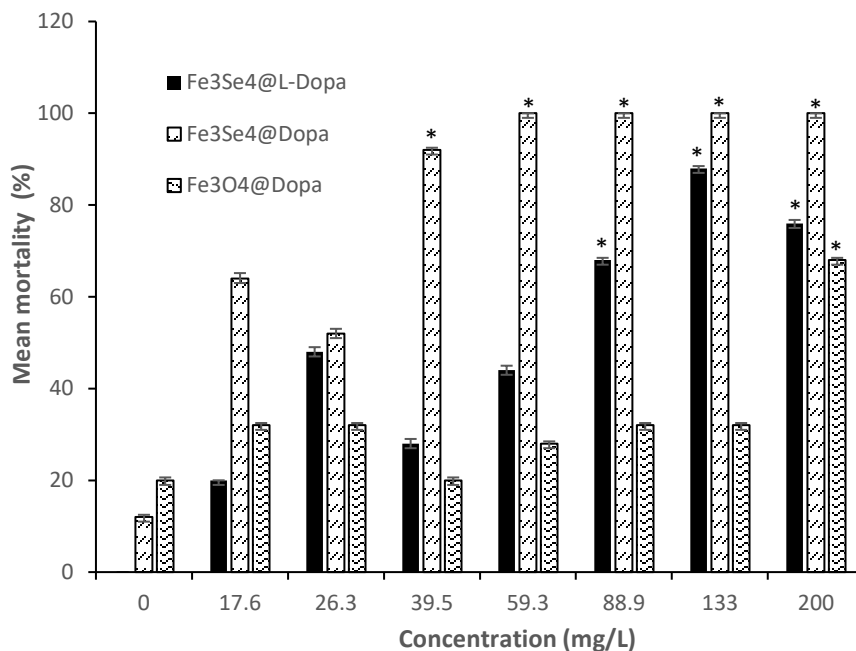


Figure 26. Average mortality of *Brachionus calyciflorus* after a 24-h exposure period to three iron nanoparticles (Iron selenide coated with Levodopamine – $Fe_3Se_4@L-Dopa$; and Iron oxide coated with Dopamine - $Fe_3O_4@Dopa$). Error bars correspond to the standard deviation; *indicates significant differences relatively to the respective control (Dunnett's; $p < 0.05$).

96-hour acute assay with *Hydra viridissima*

Mortality of *H. viridissima* after being exposed to the three iron nanoparticles was always below 9%. Malformations (including whitening of tentacles tips, clubbed/shortened tentacles and/or body slightly contracted) were only observed in hydras exposed to $Fe_3Se_4@Dopa$ (Fig. 26, 27). The highest percentage of organisms with malformations was registered at the four lowest tested concentrations (50, 77, 89, 102 mg/L) (Fig. 76).

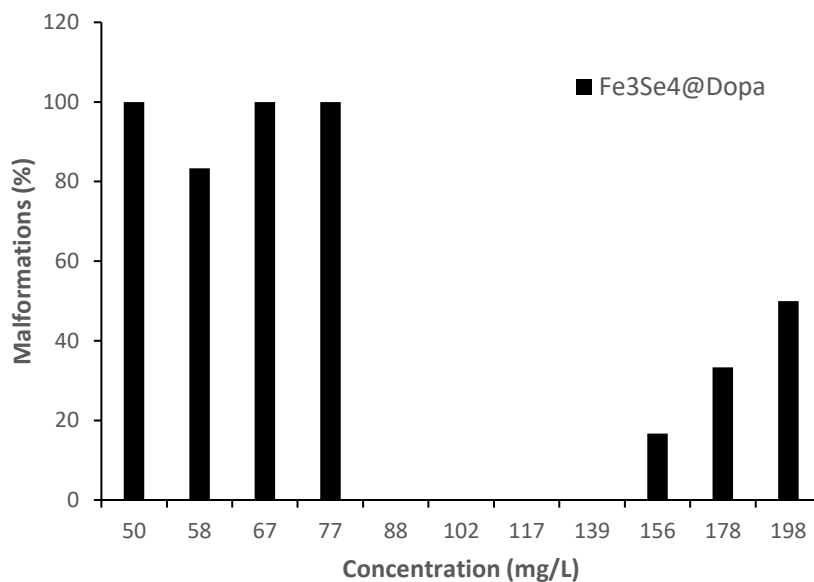


Figure 27. Percentage of malformations in *Hydra viridissima* after a 96-h exposure period to iron selenide coated with Dopamine - $Fe_3Se_4@Dopa$.

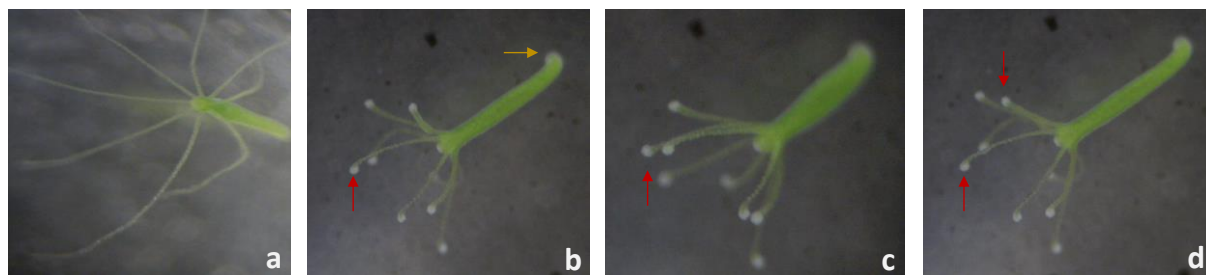


Figure 28. Images of *Hydra viridissima*; a) healthy *Hydra viridissima* hydranth; b to d) malformations detected on *Hydra viridissima* hydranths exposed to iron selenide nanoparticles coated with dopamine ($Fe_3Se_4@Dopa$) at a concentration of 88 mg/L. Red arrows represent cubbed tentacles and loss of endosymbiotic algae cells and the yellow arrow represent loss of endosymbiotic algae cells at the foot of the hydranth. The image was taken with a *Leyca* magnifier with an amplification of 400x times.

Hydras exposed to concentrations of $Fe_3O_4@Dopa$ above 58 mg/L ingested fewer artemia comparatively to the control (Fig. 29). For the other two nanoparticles a reduction in feeding was also observed, but significant differences were only observed for some intermediate tested concentrations: 88.7, 102 and 117 mg/L for $Fe_3Se_4@L-Dopa$; 102, 156, 178 and 198 mg/L $Fe_3Se_4@Dopa$ (Fig. 29). Regarding feeding inhibition, values of EC_{20} and EC_{50} were obtained as follows: 61.8 mg/L (could not be computed) for $Fe_3Se_4@Levadopa$; 28.5 mg/L (0-62.1) and 106.07

mg/L (77.0-135) for Fe₃Se₄@Dopa; and a value of EC₅₀ of 64.6 mg/L (106-2687) for Fe₃O₄@Dopa. For both Fe₃Se₄@Levodopa and Fe₃O₄@Dopa, values of EC₂₀ could not be calculated.

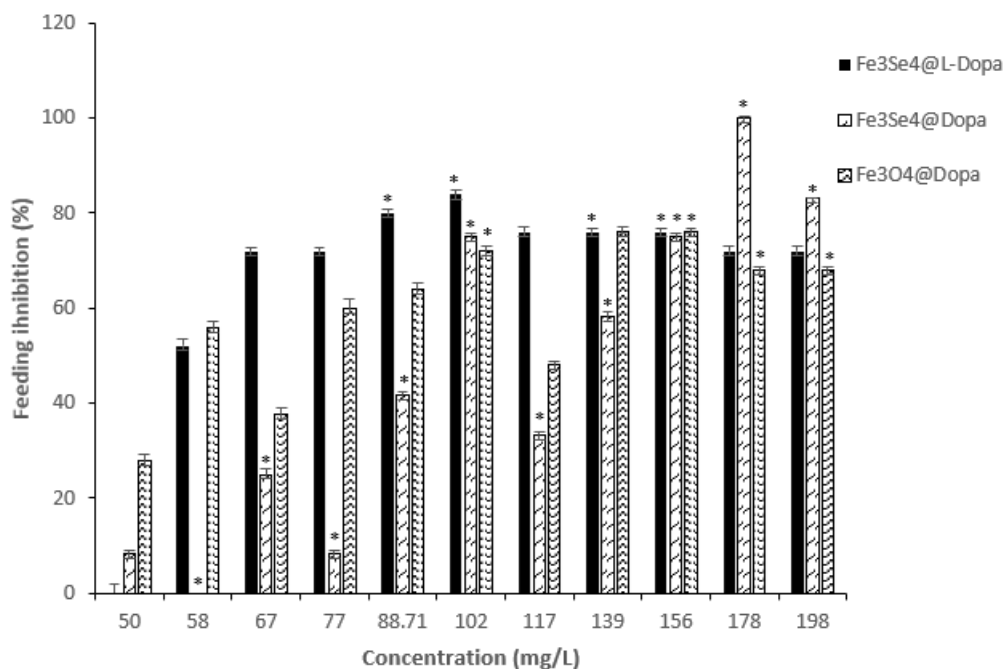


Figure 29. Average percentage of feeding inhibition of *Hydra viridissima* after a 96-h exposure period to three iron nanoparticles (iron selenide coated with levodopamine – Fe₃Se₄@L-Dopa; iron selenide coated with dopamine - Fe₃Se₄@Dopa; and iron oxide coated with dopamine - Fe₃O₄@Dopa). Error bars correspond to the standard deviation. * indicates significant differences relatively to the respective control (Dunett's; p<0.05).

96-hour embryo development assay with *Xenopus laevis*

No significant mortality occurred in embryos of *X. laevis* exposed to the two studied nanoparticles (Figs. 30, 31). Though no significant mortality occurred, it was possible to easily see NPs attached

to the eggs jelly in all tested concentrations, as well as in the egg membranes left after hatching (Fig. 32).

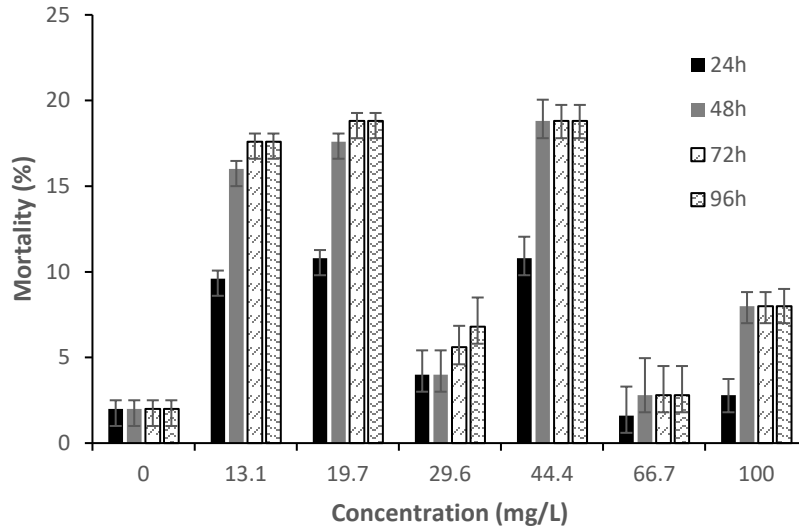


Figure 30. Average percentage of mortality of *Xenopus laevis* embryos after a 96-h exposure period to the nanoparticle of iron selenide coated with Levodopamine ($Fe_3Se_4@L-Dopa$). Error bars correspond to the standard deviation.

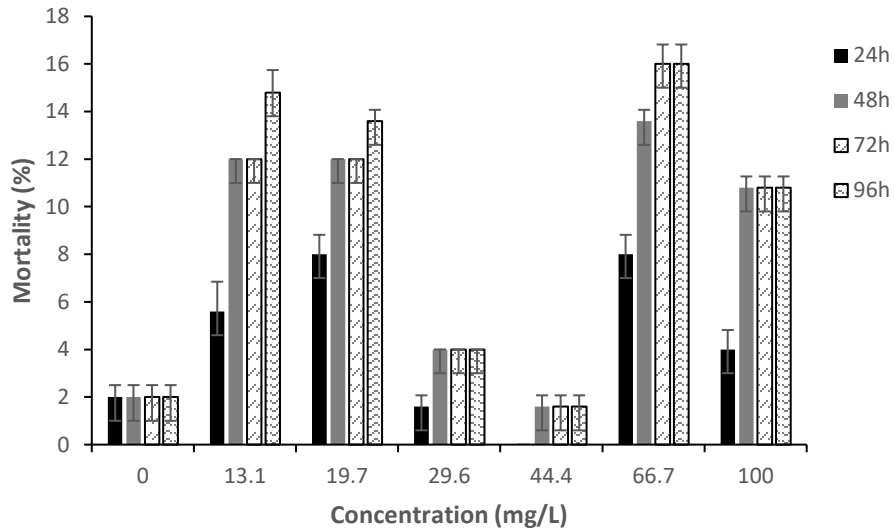


Figure 31. Average percentage of mortality of *Xenopus laevis* embryos after a 96-h exposure period to the nanoparticle of iron oxide coated with dopamine ($Fe_3O_4@Dopa$). Error bars correspond to the standard deviation.

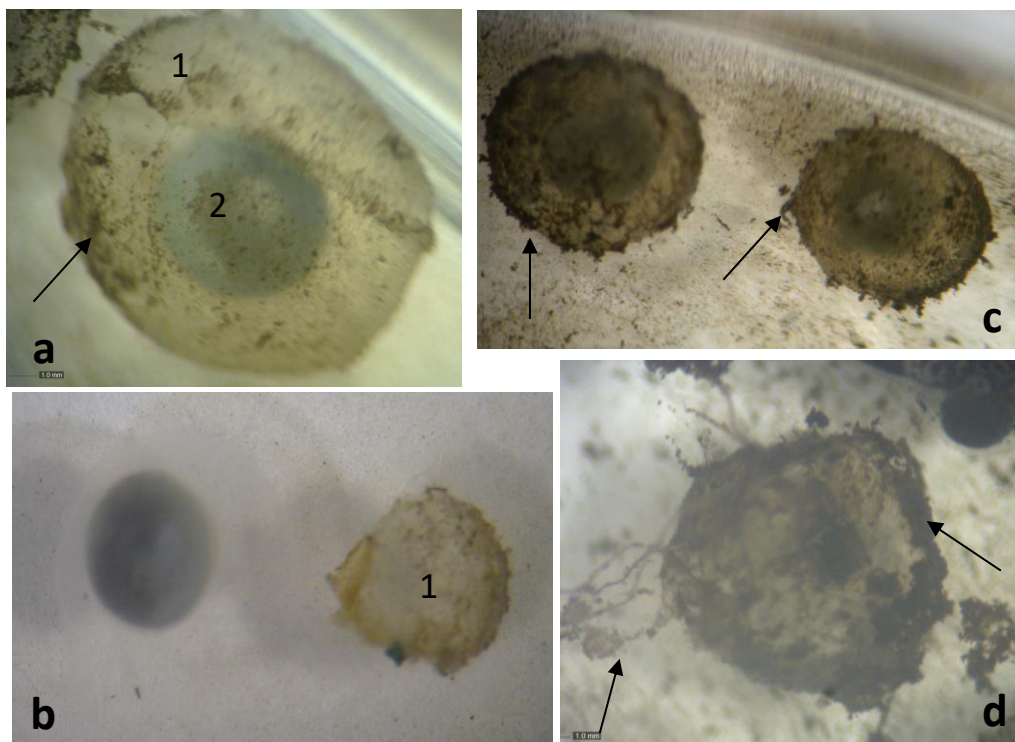


Figure 32. Embryos of the African clawed frog *Xenopus laevis* after exposure to iron oxide nanoparticles coated with levodopamine ($\text{Fe}_3\text{O}_4@L\text{-Dopa}$) at the following concentrations: a) 19.7 mg/L; b) 66 mg/L; c) and d) 100 mg/L. 1. Jelly coat that surrounds the egg; 2. Embryo. Black arrows pointing to nanoparticles adsorbed to the eggs jelly coat.

4. Discussion

4.1 Toxicity presenting ranges

The main goal of the present study intended to assess the influence of chemical composition and type of coating agent on the toxicity of iron NPs. The three NP revealed low toxicity to the tested species, since significant effects were only observed at mg/L levels. Nevertheless, when comparing toxicity among them, in general, the obtained results suggest Fe_3Se_4 to be more toxic than Fe_3O_4 NPs. This is revealed when comparing the toxicity exerted by $\text{Fe}_3\text{Se}_4@Dopa$ and $\text{Fe}_3\text{O}_4@Dopa$; the former showed to be more toxic for *L. minor*, *B. calyciflorus* and *H. viridissima*. For algae these two NPs showed similar toxicity levels ($\text{Fe}_3\text{Se}_4@Dopa$ being slightly more toxic) while for *X. laevis* any induced significant effects. Considering knowledge available in the scientific literature it would be expected that the smaller NP would be the most toxic (e.g. Pan et al., 2007; Lopes et al., 2013). Though further measurements need to be done on the studied NPs suspended in the tested media to draw more accurate conclusions, the primary size of Fe_3Se_4

NPs (56.1 to 350 nm) was larger than that of Fe₃O₄ NPs (17 to 24 nm). In addition, Fe₃Se₄ also exhibited the lowest value of zeta potential, thus being expected to further aggregate, due to Van der Waals inter particle attractions. So, the obtained results show the largest NP to be the most toxic for the tested species. One explanation for these results could involve the mechanisms of cell internalization of NPs once inside the organism. Zhao et al. (2014), reported that 100 nm-mesoporous silica NP adsorbed to the cell membranes without causing any disturbance on the membrane or cell morphology, however, larger mesoporous silica NPs (~600 nm) induced membrane deformations that were followed by internalization of the NPs. This could be a process occurring in the present work with the tested iron NPs. Furthermore, for rotifers and hydras, larger NPs (350 nm) would be easier to grab and ingest, comparatively to NPs sizing 24 nm. Adding to this, the differential chemical composition of Fe₃Se₄ and Fe₃O₄, may have also contributed to their different toxicity. Selenite has been shown to induce toxicity to several aquatic biota species at µg/L levels. The swimming speed of the ciliate *Tetrahymena pyriformis* was significantly reduced at 5 µg/L and completely stopped at 30 µg/L (Boove, 1978); Pratt and Bowers (1990) reported a 20% decrease in protozoan richness after exposure to >80 µg/L of Se. The dissociation of iron NPs in aqueous media is not well studied, however, since most metal NPs have shown some dissociation when in aqueous media, it may be hypothesized that the dissociation of Se, in addition to Fe, could have contributed to the highest toxicity of Fe₃Se₄. Finally, biota could have evolved a higher tolerance to Fe₃O₄ as iron oxides occur naturally and are relatively common in nature (in the form of nano-crystals from the earth's crust or expelled by volcanoes phenomenon's; (Singh, et al., 2010)). In the case of iron selenide these are often synthesized, also a lower molecular weight (134.8 g/mol) than Fe₃O₄ (231.5 g/mol)(PubChem, 2018), could have contributed to their dissimilar toxicity.

Regarding the influence of coating molecules in the toxicity of these iron NPs, results obtained for Fe₃Se₄@Dopa and Fe₃Se₄@Levodopa must be compared. Overall the NP coated with levodopamine showed to be less toxic. The Fe₃Se₄@Levodopa only exerted higher toxicity than Fe₃Se₄@Dopa for *L. minor*. For all the other tested species it exhibited lower or similar (only for *X. laevis*) toxicity. This lower toxicity could be related with the negative surface charge of Fe₃Se₄@Levodopa (zeta potential of -20mV). Since most cellular membranes are negatively

charged, this potential can affect NPs' tendency to permeate membranes, with cationic particles generally displaying more toxicity associated with cell wall disruption (Walker, 2012).

While there is not much information on ecotoxicological works with these nanoparticles (in part because of the emergence of the area, materials and even techniques, especially in the case of iron selenide ones) the results obtained in this dissertation are comparable with other works carried out with magnetic iron oxide NPs. Although there's a restriction on which species and NPs to compare, an overview with some of them can be done. Per example, regarding *in vitro* studies Sah, S. et al. (2017) showed that when using human hepatocellular carcinoma cells, chitosan coated iron oxide (Fe_3O_4) NPs at a concentration of $123.52\mu\text{g/L}$, cells presented a 10% viability rate after 12h of exposure. Other studies were performed in human monocyte (THP-1), hepatoma (HepG2) and ovarian cancer cell lines (Zhang, L. et al., 2017)(Feng, Q. et al., 2018) with both coated with dimercaptosuccinic acid (DMSA) and uncoated NPs respectively, with sizes between 10nm to 30nm. These authors found that cells presented iron homeostasis disturbed, by internalization of the NPs, releasing iron ion on cells, resulting in cytotoxicity and obvious signs of apoptosis at the highest tested concentration ($100\mu\text{g/mL}$) after 24h incubation, for assays with human monocytes (Zhang, L. et a., 2017). In the second case with HepG2 cell line, it was found internalization of the NPs with DNA fragmentation and extreme damage at 100g/mL after 24h of exposure to uncoated Fe_3O_4 NPs reporting once again that ROS creation was the main precursor for oxidative stress and posterior cytotoxicity (Zhang, L. et al., 2017.). Regarding assays with the ovarian cancer cell lines, it was observed cellular death at extreme tested concentrations of $400\mu\text{g/mL}$ (Feng, Q. et al., 2018).

Other obtained results in assays performed on *R. subcapitata* and *Chlorella pyrenoidosa* with uncoated Fe_3O_4 NPs with 25nm in size showed values of $\text{EC}_{50}=76\text{mg/L}$ for the first species, and $\text{EC}_{50}=30\text{mg/L}$ for the second one, regarding growth inhibition (Lei, C. et al., 2016). It was also evaluated chlorophyll content and obtained a value of $\text{EC}_{50}=90\text{mg/L}$ in chlorophyll synthesis reduction (Lei, C. et al., 2016). It was observed NPs aggregation restricting light accessibility to the cells, which in turn contributed to the algal growth inhibition (Lei, C. et al., 2016). It was pointed once more that oxidative stress was the main factor for NPs toxicity.

In an assay with the rotifera species *Brachionus manjavacas* with uncoated Fe₃O₄ NPs with 15 to 20nm in size results were reported as an increase of 34% on mortality after 48h exposure, with a EC₅₀=722 mg/L (Snell, T., et al., 2009). A study with *X. laevis* with uncoated iron oxide NPs with 20 to 40nm in size reported no embryo mortality after 96h exposure but significant malformations, at concentrations lower than 1mg/L. Finally, in a study with early life stages of zebra fish (*Danio rerio*) organisms were exposed during embryonic development and results showed that concentrations above 10 mg/L of Fe₃O₄ uncoated particles with 30nm in size induced developmental toxicity on those embryos, causing mortality, malformations and hatching delay. Concentrations of 50 and 100 mg/L cause mortality of 75% and 45%, respectively at the end of the exposure time (168h). Concentrations above 10 mg/L presented significant embryo hatching delay and toxicity (Nations, S. et al., 2011).

It is interesting to note that iron oxide aged NPs on distilled water increased surface oxidation and thus decreasing the NPs toxicity to algae (Lei, C. et al., 2016). Regarding the main toxicity pathway, literature is consensual on it, being by inducing ROS creating on cells, by high Fe uptake, resulting on oxidative stress, and lately cytotoxicity (Gupta, A. et al., 2007)(Yarjanli, Z. et al., 2017).

When comparing the sensitivity of the tested species for the three NPs, the rotifer *B. calyciflorus* showed, to be the most sensitive since lethal effects ($\geq 20\%$) were observed at concentrations as low as 17.6mg/L. *Lemna minor*, showed a similar sensitivity to that of the rotifer when exposed to Fe₃Se₄@Levadopa. It was possible to observe explicitly NP internalization on rotifers and a huge number of organisms entangled on NPs aggregates which may explain their highest sensitivity. Contrarily, the amphibian species seemed to be the most tolerant species since any effects were observed at 100mg/L of any NPs. For algae, though no significant effects were detected comparatively to the control (most probably due to the high variability in the data) it must be take into consideration that effects above 28% were observed at concentrations of 75.7mg/L for the NPs coated with dopamine. The amphibian highest tolerance to the NP could result form the protective jelly coat of the eggs that prevented the entrance of the NPs into the embryo, at least until the hatching of the organisms. Malformations were also easily observed at low concentrations of NP, but only for Fe₃Se₄@Dopa, in hydras through the whitening of the tip

of their tentacles, evidencing loss of symbiose with the microalgae (*Chlorella* sp.) that confer them their green color, which are commonly associated to this species under common conditions.

5. Conclusion

The present dissertation work aimed at increasing the knowledge on the ecotoxicity of NPs used for medical purposes, more specifically their toxicity on aquatic biota and relevant concentrations where they may pose a threat for these organisms. As these NPs are largely synthesized throughout the world, its tendency to increase in the environmental matrices within the next few years (as more techniques are being developed to optimize their production/stability/toxicity) it is advisable to put more effort on the development and production of more “environmentally friend” particles. The three tested NPs only revealed toxicity when at concentrations of mg/L, which foresees a low risk to the environment. No predicted environmental concentrations values exist for these NPs. However, it is reasonable to estimate that they will occur at levels well below $\mu\text{g/L}$, since the predicted environmental concentrations for one of the most used NPs (silver NP) are within this order of magnitude.

The obtained results point to Fe₃Se₄@Levadopa to be slightly less toxic than the other two NPs. Nevertheless, further information must still be generated namely on the physical and chemical characterization of the three NPs in order to better understand their behavior in the tested media and subsequently their effects on the studied species. Despite, more insights should be given in relation to human toxicity (cellular, genetic, nephrotic, fetal, etc) and their aggregation likeliness while in use, avoiding dangerous situations like clots in the circulatory system of the patients, per example.

Bibliography

- Ali, A., Zafar, H., Zia, M., ul Haq, I., Phull, A. R., Ali, J. S., & Hussain, A. (2016). Synthesis, characterization, applications, and challenges of iron oxide nanoparticles. *Nanotechnology, Science and Applications*, 9, 49–67.
- Amatore, C. (2015). Basic concepts. *Organic Electrochemistry, Fifth Edition: Revised and Expanded*, 3–96.
- Bahadar, H., Maqbool, F., Niaz, K., & Abdollahi, M. (2016). Toxicity of nanoparticles and an overview of current experimental models. *Iranian Biomedical Journal*, 20(1), 1–11.
- Bakand, S., Hayes, A., & Dechsakulthorn, F. (2012). Nanoparticles: A review of particle toxicology following inhalation exposure. *Inhalation Toxicology*, 24(2), 125–135.
- Behrouzkhia, Z., Joveini, Z., Keshavarzi, B., Eyvazzadeh, N., & Aghdam, R. Z. (2016). Hyperthermia: How can it be used? *Oman Medical Journal*, 31(2), 89–97.
- Bonder, M. J., & Wang, X. (2009). NIH Public Access. *Small - NIH PUBLIC ACCESS*, 4(11), 1925–1929. [ic](#)
- Brohi, R. D., Wang, L., Talpur, H. S., Wu, D., Khan, F. A., Bhattarai, D., ... Huo, L. J. (2017). Toxicity of nanoparticles on the reproductive system in animal models: A review. *Frontiers in Pharmacology*, 8(SEP), 1–22.
- Busquets, M. A., Estelrich, J., & Sánchez-Martín, M. J. (2015). Nanoparticles in magnetic resonance imaging: from simple to dual contrast agents. *International Journal of Nanomedicine*, 10, 1727.
- Chen, J. Y., Wang, E. A., Cepeda, C., & Levine, M. S. (2013). Dopamine imbalance in Huntington's disease: A mechanism for the lack of behavioral flexibility. *Frontiers in Neuroscience*, 7(7 JUL), 1–14.
- Committee, A. C. R., & Contrastmedia, D. (2018). *Contrast_Media*.
- Dale, A. L., Casman, E. A., Lowry, G. V., Lead, J. R., Viparelli, E., & Baalousha, M. (2015). Modeling nanomaterial environmental fate in aquatic systems. *Environmental Science and Technology*, 49(5), 2587–2593.
- Fate, I., Of, T. P., & Contaminants, E. (n.d.). Important Fate and Transport Properties of Environmental Contaminants.
- Gaffet, E. (2011). Nanomaterials : a review of the definitions, applications, health effects. How to implement secure development Nanomatériaux : une revue des définitions, des applications, des effets sanitaires et des moyens à mettre en oeuvre pour un développement sécurisé, 12(January 2011), 648–658.
- Gatoo, M. A., Naseem, S., Arfat, M. Y., Mahmood Dar, A., Qasim, K., & Zubair, S. (2014). Physicochemical properties of nanomaterials: Implication in associated toxic manifestations. *BioMed Research International*, 2014.
- Grover, V. P. B., Tognarelli, J. M., Crossey, M. M. E., Cox, I. J., Taylor-Robinson, S. D., & McPhail, M. J. W. (2015). Magnetic Resonance Imaging: Principles and Techniques: Lessons for Clinicians. *Journal of Clinical and Experimental Hepatology*, 5(3), 246–255.
- Ho, D. N. (2014). *Magnetic Resonance Imaging and Alternating Magnetic Fields. Cancer Theranostics*. Elsevier Inc.

- Hotze, E. M., Phenrat, T., & Lowry, G. V. (2010). Nanoparticle Aggregation: Challenges to Understanding Transport and Reactivity in the Environment. *Journal of Environment Quality*, 39(6), 1909.
- Huang, X., Liu, Q., Yao, S., & Jiang, G. (2017). Recent progress in the application of nanomaterials in the analysis of emerging chemical contaminants. *Analytical Methods*, 9(19), 2768–2783.
- Jeng, H. A., & Swanson, J. (2006). Toxicity of metal oxide nanoparticles in mammalian cells. *Journal of Environmental Science and Health - Part A Toxic/Hazardous Substances and Environmental Engineering*, 41(12), 2699–2711.
- Kaur, P., Aliru, M. L., Chadha, A. S., Asea, A., Khobar, D., Road, C., & Arabia, S. (2017). HHS Public Access, 32(1), 76–88.
- Khalid, S., Shahid, M., Natasha, Bibi, I., Sarwar, T., Shah, A. H., & Niazi, N. K. (2018). A review of environmental contamination and health risk assessment of wastewater use for crop irrigation with a focus on low and high-income countries. *International Journal of Environmental Research and Public Health*, 15(5), 1–36.
- Khot, L. R., Sankaran, S., Maja, J. M., Ehsani, R., & Schuster, E. W. (2012). Applications of nanomaterials in agricultural production and crop protection: A review. *Crop Protection*, 35, 64–70.
- Kim, J., Chhour, P., Hsu, J., Litt, H. I., Ferrari, V. A., Popovtzer, R., & Cormode, D. P. (2017). Use of Nanoparticle Contrast Agents for Cell Tracking with Computed Tomography. *Bioconjugate Chemistry*, 28(6), 1581–1597.
- Laurent, S., Dutz, S., Häfeli, U. O., & Mahmoudi, M. (2011). Magnetic fluid hyperthermia: Focus on superparamagnetic iron oxide nanoparticles. *Advances in Colloid and Interface Science*, 166(1–2), 8–23.
- Mamani, J. B., Gamarra, L. F., & Brito, G. E. de S. (2014). Synthesis and characterization of Fe₃O₄ nanoparticles with perspectives in biomedical applications. *Materials Research*, 17(3), 542–549.
- Mann, R. M., Hyne, R. V., & Choung, C. B. (2010). Hormonal induction of spermiation, courting behavior and spawning in the southern bell frog, *Litoria raniformis*. *Zoo Biology*, 29(6), 774–782.
- Rentchnick, P. (1987). *Recent Results in Cancer Research* 105.
- Rim, K. T., Song, S. W., & Kim, H. Y. (2013). Oxidative DNA damage from nanoparticle exposure and its application to workers' health: A literature review. *Safety and Health at Work*, 4(4), 177–186.
- Rybski, J. A., Spier, C. M., Miller, T. P., Lippman, S. M., Mcgee, D. L., & Grogan, T. M. (1991). Prediction of outcome in diffuse large cell lymphoma by the major histocompatibility complex class II (HLA-DR, DP, DQ) and class I (HLA-a, b, c) phenotype. *Leukemia and Lymphoma*, 6(1), 31–38.
- Seeman, P., & Madras, B. (n.d.). *IMAGING OF THE HUMAN BRAIN IN HEALTH* Edited by.
- Segers, H. (2007). *Annotated checklist of the rotifers (Phylum Rotifera), with notes on nomenclature, taxonomy and distribution*. *Zootaxa*.
- Shi, S., Lu, R., Wang, T., Sun, H., & Wang, H. (1999). SYNTHESIS OF CeO₂ NANOPARTICLES IN W/ O MICROEMULSION. *Journal of Dispersion Science and Technology*, 20(4), 1247–1262.
- Stephen, Z. R., Kievit, F. M., & Zhang, M. (2012). NIH Public Access, 14(11), 330–338.
- Syslova, K., Rambousek, L., Bubenikova-Valesova, V., Slamberova, R., Novotny, P., & Kacer, P. (2012).

- Dopamine Analysis in Neuroscience Research. *Dopamine: Functions, Regulation and Health Effects*, (December 2015), 81–112.
- Tu, C., Osborne, E. A., & Louie, A. Y. (2011). Activatable T 1 and T 2 magnetic resonance imaging contrast agents. *Annals of Biomedical Engineering*, 39(4), 1335–1348.
- Viglino, L., Aboulfadl, K., Prévost, M., & Sauvé, S. (2008). Analysis of natural and synthetic estrogenic endocrine disruptors in environmental waters using online preconcentration coupled with LC-APPI-MS/MS. *Talanta*, 76(5), 1088–1096.
- Völker, C., Oetken, M., & Oehlmann, J. (2014). Reviews of Environmental Contamination and Toxicology Volume 228, 228(May 2014).
- Wu, L., Zhang, J., & Watanabe, W. (2011). Physical and chemical stability of drug nanoparticles. *Advanced Drug Delivery Reviews*, 63(6), 456–469.
- Wust, P., Hildebrandt, B., Sreenivasa, G., Rau, B., Gellermann, J., Riess, H., ... Schlag, P. (2002). Hyperthermia in combined treatment of cancer. *Lancet Oncology*, 3(8), 487–497.
- Zhao, F. Y., Li, Y. L., & Li, L. H. (2014). Preparation and Characterization of Magnetite Nanoparticles. *Applied Mechanics and Materials*, 618, 24–27.
- Zuckerberg, M. (2016). What Are Chatbots and How Do They Work, 1–9.
- American Society for Testing and Materials. 1998. Standard Guide for Conducting the Frog Embryo Teratogenesis Assay-Xenopus (FETAX). Standard Guide E1439-98. ASTM International, West Conshohocken, PA.
- N. Winterton. Green chemistry: deliverance or distraction? *Clean Technologies and Environmental Policy*, 18(4):991–1001, Apr 2016.
- E. D. Smolensky, H. E. Park, T. S. Berquó, and V. C. Pierre. Surface functionalization of magnetic iron oxide nanoparticles for mri applications – effect of anchoring group and ligand exchange protocol. *Contrast Media and Molecular Imaging*, 6(4):189–199.
- R. M. Patil, N. D. Thorat, P. B. Shete, P. A. Bedge, S. Gavde, M. G. Joshi, S. A. M. Tofail, and R. A. Bohara. Comprehensive cytotoxicity studies of superparamagnetic iron oxide nanoparticles. *Biochem Biophys Rep*, 13:63–72, Mar 2018.
- O. Zvarec, S. Purushotham, A. Masic, R. V. Ramanujan, and A. Miserez. Catecholfunctionalized chitosan/iron oxide nanoparticle composite inspired by mussel thread coating and squid beak interfacial chemistry. *Langmuir*, 29(34):10899–10906, 2011.
- J. Chen, Z. Fang, P. Lie, and L. Zeng. Computational lateral flow biosensor for proteins and small molecules: A new class of strip logic gates. *Analytical Chemistry*, 84(15):6321–6325, 2012.
- W. Wang, Y. Dai, H. Zhang, H. Luo, and Y. Chen. Preparation and characterization of superparamagnetic iron oxide nanoparticle-graphene oxide nanocomposites. *Journal of Nanoscience and Nanotechnology*, 16(7):7159–7163, 2016.

- Y Pan, S Neuss, A Leifert, M Fischler, F Wen, U Simon, G Schmid, W Brandau, W Jahnen-Dechent. 2007. Size-Dependent Cytotoxicity of Gold Nanoparticles. *Small* 11: 1941 – 1949.
- S Lopes, F Ribeiro, J Wojnarowicz, K Jurschat, A Crossley, AMVM Soares, S Loureir. 2013. Zinc oxide nanoparticles toxicity to *Daphnia magna*: size-dependent effects and dissolution.
- Zhao Y, Sun X, Zhang G, Trewyn BG, Slowing II, Lin VS. Interaction of mesoporous silica nanoparticles with human red blood cell membranes: size and surface effects. *ACS Nano*. 2011;5:1366–1375.
- Bovee EC. 1978. Effects of heavy metals especially selenium, vanadium and zirconium on movement, growth and survival of certain animal aquatic life. PB-292563. Arlington (VA, USA): National Technical Information Service, 26 pp.
- Pratt JR, NJ Bowers. 1990. Effect of selenium on microbial communities in laboratory microcosms and outdoor streams. *Tox. Assess* 5:293 -308.
- Feng, Q., Liu, Y., Huang, J., Chen, K., Huang, J., & Xiao, K. (2018). Uptake, distribution, clearance, and toxicity of iron oxide nanoparticles with different sizes and coatings. *Scientific Reports*, 8(1), 1–13.
- Gupta, A. K., Naregalkar, R. R., Vaidya, V. D., & Gupta, M. (2007). Recent advances on surface engineering of magnetic iron oxide nanoparticles and their biomedical applications. *Nanomedicine*, 2(1), 23–39.
- Lei, C., Zhang, L., Yang, K., Zhu, L., & Lin, D. (2016). Toxicity of iron-based nanoparticles to green algae: Effects of particle size, crystal phase, oxidation state and environmental aging. *Environmental Pollution*, 218, 505–512.
- Nations, S., Wages, M., Cañas, J. E., Maul, J., Theodorakis, C., & Cobb, G. P. (2011). Acute effects of Fe 2O₃, TiO₂, ZnO and CuO nanomaterials on *Xenopus laevis*. *Chemosphere*, 83(8), 1053–1061.
- Shah, S. N. A., Shah, Z., Hussain, M., & Khan, M. (2017). Hazardous Effects of Titanium Dioxide Nanoparticles in Ecosystem. *Bioinorganic Chemistry and Applications*, 2017.
- Singh, N., Jenkins, G. J. S., Asadi, R., & Doak, S. H. (2010). Potential toxicity of superparamagnetic iron oxide nanoparticles (SPION). *Nano Reviews*, 1(1), 5358.
- Tinsley, R., Minter, L., Measey, J., Howell, K., Veloso, A., Núñez, H. & Romano, A. 2009. *Xenopus laevis*. *The IUCN Red List of Threatened Species* 2009: e.T58174A11730010
- Walker, J. M. (2012). *Methods in Drug Design and Discovery*.
- Yarjanli, Z., Ghaedi, K., Esmaili, A., Rahgozar, S., & Zarrabi, A. (2017). Iron oxide nanoparticles may damage to the neural tissue through iron accumulation, oxidative stress, and protein aggregation. *BMC Neuroscience*, 18(1), 1–12.
- Zhang, L., Xie, H., Liu, Y., & Wang, J. (2017). Research on Nanotoxicity of an Iron Oxide Nanoparticles and Potential Application. *Toxicology: Open Access*, 03(03), 1–7.

Annexes

Annex 1 - Microalgae medium (MBL) (OECD 201, 2006)

	Chemical composition	Quantity of compound for stock solution (g/L)	Volume of stock solution per L of milli-Q water (mL)
Macronutrients	CaCl ₂ ·2H ₂ O	36,76	1
	MgSO ₄ ·7H ₂ O	36,97	1
	NaHCO ₃	12,6	1
	K ₂ HPO ₄	8,71	1
	NaNO ₃	85,01	1
	NaSiO ₃ ·9H ₂ O	28,42	1
Micronutrients	Na ₂ EDTA	4,36	1
	FeCl ₃ ·6H ₂ O	3,15	1
	CuSO ₄ ·5H ₂ O	0,001	1
	ZnSO ₄ ·7H ₂ O	0,022	1
	CoCl ₂ ·6H ₂ O	0,01	1
	MnCl ₂ ·4H ₂ O	0,18	1
	Na ₂ MoO ₄ ·2H ₂ O	0,006	1
Vitamins (*)	Tiamina HCl (B ₁)	0,1mg/L	
	Biotina (H)	0,5mg/L	
	Cianocobalamina (B ₁₂)	0,5mg/L	
	TRIS (hidroximetil aminometano)	50g/200mL	2

(*) added ONLY after sterilization and with the medium cold

Annex 2 - Macrophytes medium (Steinberg) (OECD 221, 2006)

Stock solution No.	Substance	Concentration in stock solution (g·l ⁻¹)	Concentration in prepared medium (mg·l ⁻¹)	Prepared medium	
				Element	Concentration (mg·l ⁻¹)
I	NaNO ₃	8.50	85	Na ; N	<u>32 ; 14</u>
	KH ₂ PO ₄	1.34	13.4	K ; P	<u>6.0 ; 2.4</u>
II	MgSO ₄ · 7H ₂ O	15	75	Mg ; S	<u>7.4 ; 9.8</u>
III	CaCl ₂ · 2H ₂ O	7.2	36	Ca ; Cl	<u>9.8 ; 17.5</u>
IV	Na ₂ CO ₃	4.00	20	C	<u>2.3</u>
V	H ₃ BO ₃	1.0	1.00	B	<u>0.17</u>
	MnCl ₂ · 4H ₂ O	0.20	0.20	Mn	<u>0.056</u>
	Na ₂ MoO ₄ · 2H ₂ O	0.010	0.010	Mo	<u>0.0040</u>
	ZnSO ₄ · 7H ₂ O	0.0050	0.0050	Zn	<u>0.011</u>
	CuSO ₄ · 5H ₂ O	0.010	0.010	Cu	<u>0.0013</u>
	Co(NO ₃) ₂ · 6H ₂ O			Co	<u>0.0020</u>
VI	FeCl ₃ · 6H ₂ O	0.17	0.84	Fe	<u>0.17</u>
	Na ₂ -EDTA · 2H ₂ O	0.28	1.40	-	-
VII	MOPS (buffer)	490	490	-	-

Annex 3 - Rotifers medium (Rotokit F chronic, Microbiotests, Gent, Belgium)

<p>ROTOX_{freshwater}/OSTRACODTOX Medium (freshwater rotifers – <i>Brachionus calyciflorus</i> and ostracods – <i>Heterocypris incongruens</i>)</p> <p>For each Liter:</p> <p>96 mg of NaHCO₃ - n°62</p> <p>60 mg of CaSO₄.2H₂O - n°93</p> <p>60 mg of MgSO₄.7H₂O - n°96</p> <p>4 mg of KCl - n°44</p>

Annex 4 - Hydra Medium (Trottier, S. et al., 1997)

Calcium chloride, CaCl ₂ · 2H ₂ O	2.94 g
N-tris [hydroxymethyl]methyl 1-2-aminoethanesulfonic acid (TES buffer)	2.2 g
Ethylenediaminetetraacetic acid (EDTA)	0.080 g
Ultrapure water	20.0 L

Annex 5 - Amphibians medium (FETAX) (OECD, 2008)

FETAX Medium (20L)				
Ultra pure or deionized water				
Composto	Forma Existente	Nr Reagente	Quantidade (mg) para 20L	pH
NaCl	-	46	1250	8,00
NaHCO ₃	-	62	1920	
Kcl	-	44	600	
CaCl ₂	CaCl ₂ .2H ₂ O	37	468	
CaSO ₄ .2H ₂ O	-	93	1200	
MgSO ₄	MgSO ₄ .7H ₂ O	96	2901	

Annex 6 – Resume table for L(E)C_x obtained values

L(E)C _x (in mg/L, with 95% CL) or Highest % of effect at the highest tested concentration							
Species	Endpoint	L(E)C ₂₀			L(E)C ₅₀		
		Fe ₃ Se ₄ @L-Dopa	Fe ₃ Se ₄ @Dopa	Fe ₃ O ₄ @Dopa	Fe ₃ Se ₄ @L-Dopa	Fe ₃ Se ₄ @Dopa	Fe ₃ O ₄ @Dopa
<i>R. subcapitata</i>	Growth rate	(n.d.)	(n.d.)	(n.d.)	No effect	No effect	No effect
	Yield	(n.d.)	(n.d.)	(n.d.)	(n.d.)	(n.d.)	(n.d.)
<i>L. minor</i>	Growth rate	(n.d.)	125.88	199.50	23	142.82	203.49
	Chl a	(n.d.)	(n.d.)	157.66	(n.d.)	(n.d.)	208.44
	Chl b	(n.d.)	155.94	(n.d.)	(n.d.)	(n.d.)	202.53
	Chl a+b	(n.d.)	142.39	(n.d.)	(n.d.)	(n.d.)	205.67
<i>B. calyciflorus</i>	Mortality	15.43	10.42	12.48	50.6	18.7	239
<i>H. viridissima</i>	Morphology	No effect	(n.d.)	No effect	No effect	178	No effect
	Feeding	(n.d.)	28.45	(n.d.)	61.8	106.1	64.6
<i>X. laevis</i>	Mortality	(n.d.)	(n.d.)	(n.d.)	8% at 100	(n.d.)	(n.d.)